Historical snow and ice temperature observations document the recent warming of the Greenland ice sheet

Baptiste Vandecrux[1], Robert S. Fausto[1], Jason E. Box[1], Federico Covi[2], Regine Hock[2, 3], Asa K. Rennermalm[4], Achim Heilig[5], Jakob Abermann[6], Dirk van As[1], Elisa Bjerre[7], Xavier Fettweis[8], Paul C.J.P. Smeets[9], Peter Kuipers Munneke[9], Michiel R. van den Broeke[9], Max Brils[9], Peter L. Langen[10], Ruth Mottram[11], Andreas P. Ahlstrøm[1]

[1]Geological Survey of Denmark and Greenland (GEUS), Department of Glaciology and Climate, Copenhagen, Denmark
[2]Geophysical Institute, University of Alaska Fairbanks, Fairbanks, AK, USA
[3]Department of Geoscience, University of Oslo, Oslo, Norway
[4]Department of Geography, Rutgers, the State University of New Jersey, Piscataway, NJ, USA
[5]Department of Earth and Environmental Sciences, Ludwig Maximilian University, Munich, Germany
[6]Department of Geography and Regional Sciences, University of Graz, Heinrichstraße 36, 8010, Graz, Austria
[7]Department of Geosciences and Natural Resource Management (IGN), University of Copenhagen (UCPH), Øster Voldgade 10, DK-1350 Copenhagen, Denmark
[8]Geography, University of Liège, Liège, Belgium
[9]Institute for Marine and Atmospheric Research, Utrecht University, Utrecht, the Netherlands
[10]Department of Environmental Science, iClimate, Aarhus University, Roskilde, Denmark
[11]Danish Meteorological Institute, Copenhagen, Denmark

Correspondence to: Baptiste Vandecrux (bav@geus.dk)

Abstract

The surface melting of the Greenland ice sheet has been increasing over the last decades due to Arctic atmospheric warming. Surface melt depends on the energy balance which includes the atmospheric forcing but also the thermal budget of the snow, firn and ice near the ice sheet surface. We present a compilation of more than 4500 measurements of ice, snow and firn temperature at 10 m below the surface (T_{10m}) across Greenland spanning from 1912 to 2022. The measurements are either instantaneous or monthly averages. We train an Artificial Neural Network model (ANN) on these observations, weighted by their relative representativity, and use it to reconstruct T_{10m} over the entire Greenland ice sheet. We use 10 year averages and mean annual values of air temperature and snowfall from the ERA5 reanalysis dataset (1950-2022) as model input. The ANN indicates a Greenland-wide positive trend of T_{10m} at 0.2 ℃ decade^{-1} during the 1950-2022 period, with a cooling during 1950-1985 (-0.3 ℃ decade^{-1}) followed by a warming during 1985-2022 (+0.7 ℃ decade^{-1}). Regional climate models HIRHAM5, RACMO2.3p2 and MARv3.12 show mixed results compared to the observational T_{10m} dataset with mean differences ranging from -0.4 ℃ (HIRHAM) to 1.3 ℃ (MAR) and root mean squared differences ranging from 2.8 ℃ (HIRHAM) to 4.7 ℃ (MAR). The corresponding values for the ANN are -0.2 ℃

35   and 1.7 °C. The observation-based ANN also reveals an underestimation of the subsurface warming trends in
climate models for the bare ice and dry snow areas. The subsurface warming brings the Greenland ice sheet
surface closer to the melting point, reducing the amount of summer energy input required for melting. Our
compilation documents the response of the ice sheet subsurface to atmospheric warming and will enable further
improvements of models used for ice sheet mass loss assessment and reduce the uncertainty in projections.

40   **1.   Introduction**

The Arctic is warming more than four times as fast as the global average (Chylek et al., 2022, Rantanen et al.,
2022). Consequently, the Greenland ice sheet is undergoing an increase in air temperature (e.g. Hanna et al.,
2021, Zhang et al., 2022) and increased anticyclonic, cloud free conditions in summer (Hofer et al., 2017; Ryan et
al., 2022). In the low elevation bare ice area of the ice sheet, the warming atmosphere increases the heat transfer
45   to the surface through turbulent heat fluxes (e.g., Wang et al. 2021), while a reduction in cloud cover increases
the downward shortwave radiation, both resulting in melt increases since the late 1980s (Hofer et al., 2017,
Trusel et al., 2018, Ryan et al., 2022). Enhanced melt in the bare ice area initiates multiple feedback processes,
such as snowline retreat (Noël et al., 2019; Ryan et al., 2019) and algal growth (e.g. Stibal et al., 2017; Cook et
al., 2020), which lead to further expansion and darkening of the bare ice area and enhanced shortwave radiation
50   absorption. At higher elevations, increased surface melt also triggers a melt-albedo feedback through which
liquid water within snow decreases the snow albedo and increases the absorption of solar radiation (e.g. Box et
al., 2012). The increase in ice sheet surface energy influx leads to an increase in surface melt but also to an
increase of subsurface temperatures through heat conduction and refreezing of meltwater (Polashenski et al.,
2014, McGrath et al., 2013). The subsurface temperature is therefore a key indicator of how the Greenland ice
55   sheet has been affected by recent climatic changes. Furthermore, ice sheet subsurface warming brings the near-
surface snow and firn (multi-year, compressed snow) closer to the melting point and makes them less efficient at
retaining meltwater (Pfeffer et al., 1991; Vandecrux et al., 2020a). Subsurface warming could also trigger thermal
regime shifts across the ice sheet (Marshall, 2021), increased ice flow and subsequent dynamic mass loss
(Phillips et al., 2010, 2013, Colgan et al., 2015).

60

Over the last century, research teams have reported snow, ice and firn subsurface temperatures of the Greenland
ice sheet. Here, we compile a dataset of 4615 observations of ice, snow and firn temperature at 10 m below the
surface (T_{10m}) spanning from 1912 to 2022 from published and unpublished sources. We then use 4600

observations of T_{10m} within the current ice sheet extent and the period 1950-2022 to train an Artificial Neural
Network (ANN) model that can predict T_{10m} over the entire ice sheet. For a given month and location, the ANN
estimates T_{10m} based on 14 parameters derived from the ERA5 reanalysis (Hersbach et al., 2020) and representing
the long term and recent history of air temperature and snowfall. Using our observational dataset of subsurface
temperature as well as our ANN, we evaluate three regional climate models widely used to estimate the surface
mass balance of the Greenland ice sheet: RACMO2.3p2 coupled to an offline firn model IMAU-FDM v1.2G
(hereafter RACMO, Noël et al., 2019, Brils et al., 2022), MARv3.12 (hereafter MAR, Fettweis et al., 2017, 2020)
and HIRHAM5 (hereafter HIRHAM, Langen et al., 2017). We put special emphasis on T_{10m} magnitude and
trends in various areas of the ice sheet. Lastly, we discuss the impact of this subsurface warming on the ice sheet
mass balance processes.

2. Methods

2.1. Observed ice sheet subsurface temperature compilation and interpolation

A total of 4615 T_{10m} observations were compiled from 48 sources (Figure 1, Table 1). Each dataset is described in
the related reference in Table 1, except two yet undescribed datasets. The first unpublished dataset was collected
by the late K. Steffen and his team and consists of two thermistor strings, one at Swiss Camp, central western
Greenland, and another at Summit station, central Greenland, to complement the Greenland Climate Network
(GC-Net) automated weather stations (AWS) at those sites (Steffen et al., 1996, 2001). The 11 m long string at
Swiss Camp was operating between 1992 and 2009 and equipped with UUB thermistors at 0.5, 0.75 m depth and
1-11 m depth with 1 m spacing. The 10 to 15 m long string at Summit was equipped with Campbell Scientific
T107 thermistors and active during the periods 2000-2002 and 2007-2009. New sensors were added to the
Summit string along the years. The sensors' depth and surface height evolution could be recovered from field
notes and this data is now presented for the first time. The second yet unpublished dataset comes from 14 new
AWS installed in 2021 and 2022 by the Geological Survey of Denmark and Greenland (GEUS) as a continuation
of the GC-Net sites (Steffen et al., 1996, 2001, Vandecrux et al., 2023). They are equipped with 11 GeoPrecision
TNode thermistors on a string installed down to 10 m. These data are hosted on the same dataset as the
PROMICE AWS data (How et al., 2022).

We also post-processed two previously published datasets. The data from Humphrey et al. (2012) was corrected
for the changing depth of the sensor below the surface as snow accumulates or melts at the surface

(Supplementary Text 1) - similar to the processing of the other time series. The FirnCover dataset (MacFerrin et al., 2022) appeared to have a warm bias due to the use of uncalibrated resistance temperature detectors instead of
95   the conventional thermistor or thermocouple instruments. Using as reference the firn temperature observations reported by Samimi et al. (2021) and Heilig et al. (2018) at DYE-2, we built an ad-hoc correction function that was then applied at all sites within the FirnCover dataset. The correction procedure is described in Supplementary Text 2 and reduces the FirnCover temperatures by 1.1 °C on average.

100   For the temperatures continuously recorded by thermistor or thermocouple strings, the depth of each temperature sensor below the surface was calculated using installation depths and recorded surface height. Wherever necessary, we interpolated the available temperature profiles linearly to 10 m depth and allowed linear extrapolation if at least two measurements were available within 2 m of the 10 m depth. The resulting T_{10m} values were then aggregated as monthly means if they originated from continuous measurements or left as instantaneous
105   values otherwise. Seven T_{10m} was found to be outside of the current ice sheet extent: the five measurements from Koch (1913) and two measurements from Benson (1962). The latter could not be used for the training of the ANN.

The measurements conducted by different scientific teams at the same location allow for an assessment of
110   uncertainty and reproducibility of "local" vertically interpolated T_{10m} observations. From 10 sites where simultaneous measurements are available, the median root mean square difference (RMSD) is 0.5 °C (Supplementary Table 1).
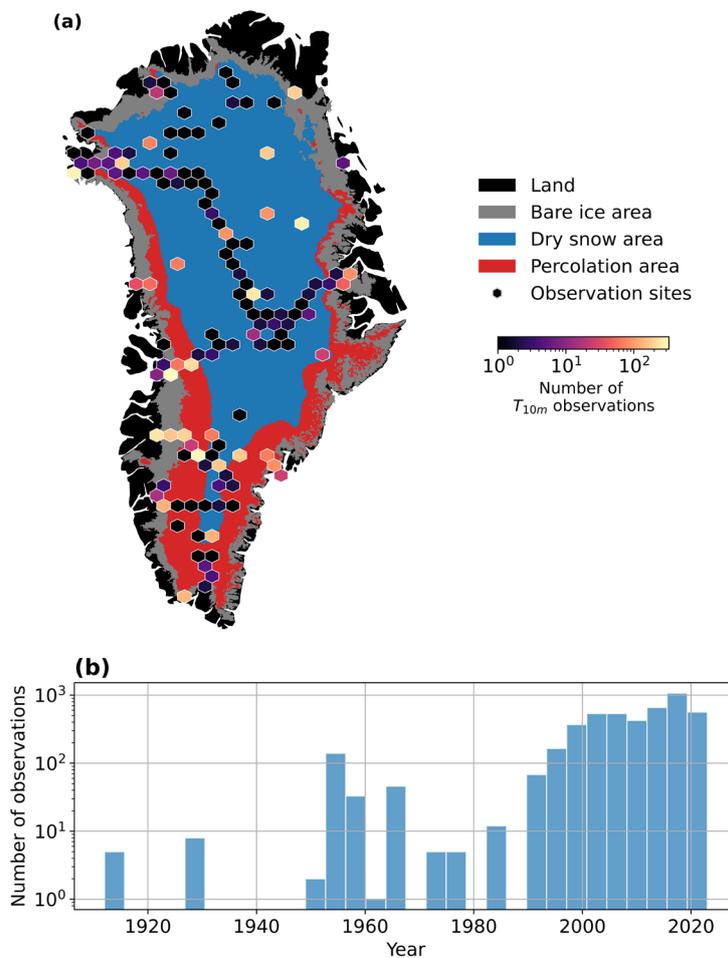
Figure 1. Spatial (a) and temporal (b) distribution of the T_{10m} observations in Greenland. Greenland surface classification according to Vandecrux et al. (2019) based on firn density profiles and remote sensing observations.

Table 1. Overview of T_{10m} datasets used in this study. Bold number of measurements indicate the number of monthly averages derived from the original measurements.

Reference	Start year	End year	Number of measurements
Koch (1913)	1912	1913	5
Wegener (1930); Abermann et al. (2023)	1930	1930	8
Heuberger (1954)	1950	1950	2
Benson (1962)	1954	1955	59
Schytt (1955)	1954	1954	31
Nobles (1960)	1954	1954	7

Heuberger (1954)	1954	1954	1
Meier et al. (1957)	1955	1955	4
Griffiths (1960)	1955	1956	38
de Quervain (1969)	1957	1964	8
Ambach (1979)	1959	1959	2
Langway (1961)	1959	1959	14
U.S. Army Transportation Board (1960)	1960	1960	4
Davis (1954)	1960	1960	7
Davis (1967)	1962	1962	1
Mock (1965)	1964	1964	12
Mock and Ragle (1963)	1964	1964	31
Weertman et al. (1968)	1966	1966	1
Colbeck and Gow (1979)	1973	1973	3
Clausen et al. (1988)	1974	1985	11
Clausen and Hammer (1988)	1977	1977	1
Stauffer and Oeschger (1979)	1978	1978	3
Clement (1984)	1983	1983	4
Thomsen et al. (1991)	1990	1991	8
Ohmura et al. (1992)	1990	1990	3
GC-Net unpublished	1991	2010	**170**
Braithwaite (1993)	1991	1992	12
Laternser (1994)	1992	1992	16
Schwager (2000)	1994	1994	1
Historical GC-Net: Steffen et al. (1996, 2001, 2023); Vandecrux et al. (2023)	1995	2022	**1665**
Giese and Hawley (2015)	2004	2008	**47**
Humphrey et al. (2012)	2007	2009	**57**
PROMICE: Fausto et al. (2021); How et al. (2022)	2008	2023	**1319**
Smeets et al. (2018)	2009	2016	**160**
Harrington et al. (2015)	2010	2012	5
Hills et al. (2018)	2011	2017	**109**
Charalampidis et al. (2016); Charalampidis et al. (2022)	2012	2013	**29**
Yamaguchi et al. (2014)	2012	2012	1
Miller et al. (2020)	2013	2017	**68**
Polashenski et al. (2014)	2013	2013	2

Matoba et al. (2015)	2014	2014	1
MacFerrin et al. (2021, 2022)	2015	2019	**311**
Kjær et al. (2015)	2015	2015	2
Heilig et al. (2018)	2016	2021	**58**
Vandecrux et al. (2021); Colgan and Vandecrux (2021)	2017	2022	**119**
Covi et al. (2022, 2023)	2017	2019	77
Law et al. (2021)	2019	2019	1
GC-Net continuation: Fausto et al. (2021); How et al. (2022)	2021	2023	**117**
		Total:	4615

120

2.2. The artificial neural network

T_{10m} is predominantly controlled by 1) the surface temperature through molecular heat conduction, 2) the subsurface refreezing of meltwater through latent heat release, and 3) snowfall rates which determine the vertical advection velocity in the firn column. The near-surface air temperature can act as a proxy for both surface

125 temperature and surface melt in the absence of reliable estimates, because they all interact within the surface energy budget. The surface temperature itself depends on the near-surface air temperature through turbulent heat fluxes and the surface energy budget. This relationship between air temperature, snowfall and T_{10m} is notably non-linear: in regions where surface melt is common, meltwater refreezing at depth will lead to T_{10m} several degrees higher than the average air temperature (e.g. Humphrey et al, 2012). On the other hand, during periods of

130 minimal or no melting in the summer, the radiative imbalance at the surface and the presence of a near-surface atmospheric inversion can cause the subsurface temperatures to be several degrees lower than the near-surface air temperature (e.g. Miller et al., 2017). ANNs have proven their ability to capture these non-linearities and interactions between input parameters in numerous glaciological and meteorological applications (e.g. Steiner et al., 2005, Braakmann-Folgmann and Donlon, 2019, Xu et al., 2021). Given that our training data does not

135 encompass all possible ice sheet conditions, we favor ANNs over tree-based algorithms that can be limited when used beyond their training dataset (e.g., Xiong et al., 2020, Liu et al., 2022). Finally, during our search for the most straightforward ANN structure capable of modeling our dataset, we ultimately chose a multi-layer perceptron (Rumelhart et al. 1986). We want to highlight that the choice of model structure, input parameters and training strategy does not have a single optimal configuration. Some of our choices are even decreasing the

140 apparent performance of the model in order to avoid overfitting and to increase the model's capacity to

extrapolate outside of its training set. The following sections describe selection of inputs, our enhancement of the dataset's representativity and eventually the ANN structure, training and uncertainty assessment.

2.2.1. The input parameters

We use the air temperature and snowfall monthly grids from the ERA5 reanalysis (Hersbach et al., 2020): either
145   from ERA5 Land at spatial resolution 0.1x0.1° for 1950-2022 (Muñoz Sabater, 2019) or from the original ERA5 (Hersbach et al., 2023) at 0.25x0.25° resolution, resampled linearly to 0.1x0.1° for 1940-1950. The 10 year average temperature ($\overline{T_{2m,10\,y}}$) and snowfall ($\overline{SF_{10\,y}}$) were calculated for each cell and each month to represent the long term conditions at a given time and place. Additionally, we calculate for each grid cell and monthly time step the amplitude of the 2 m air temperature in the previous year ($T_{2m,\,amp}$) as well as the average air temperature
150   and snowfall of the five previous years. This reflects the capacity of the subsurface to respond, not only to changes in long term changes, but also to recent changes in air temperatures and snowfall (e.g. Polashenski et al., 2014). Lastly, we give as input the cosine of the month (giving 1 in January and -1 in July) to assist the ANN in capturing the annual periodicity. For a given time and location, the ANN therefore takes 14 inputs: $\overline{T_{2m,10\,y}}$, $\overline{SF_{10\,y}}$ and $T_{2m,\,amp}$, the five previous years of annual snowfall, the five previous years of air temperature and the
155   month.

2.2.2. Weighing of the observations prior to ANN training

Many machine learning algorithms, including ANN, assume that the training data are representative of the target area (where the model is applied for predictions), i.e., that the data are drawn from the same distribution. This assumption is violated in practice when applying the model to new spatial domains that may contain local
160   conditions not present in the training data. Thus, the representativity of the training dataset compared to the target area is critical for the robustness of any machine learning model, i.e. how well the model generalizes to new and unseen data (Meyer and Pebesma, 2021; Bjerre et al., 2022). The representativity of the 4600 observation sites (training data) compared to the entire Greenland ice sheet where the ANN will be applied (target area) was quantified using histogram analysis (Figure 2). For the three input parameters that define the climate at a given
165   location ($\overline{T_{2m,10\,y}}$, $\overline{SF_{10\,y}}$ and $T_{2m,\,amp}$), here referred to as $p_{i\,=\,1,\,2,\,3}$, we plot the probability histogram of the parameter p_i as it appears in ERA5 at our observation locations: this is the 'observation' histogram $H_o(p_i)$. We then plot, for that input parameter p_i, the probability histogram of all the ice sheet pixels, and all time steps within the ERA5 dataset: this is the 'target' histogram $H_t(p_i)$. The 'observation' histograms $H_o(p_i)$ represent the distribution the ANN will learn from while the 'target' histograms $H_t(p_i)$ represent the values over which the

170 ANN will eventually be applied (Figure 2). In an ideal scenario where the observational dataset is representative
of the parameter space where the ANN will be applied, $H_o(p_i)$ and $H_t(p_i)$ should show similar distributions. We
evaluate this similarity with the Canberra distance (Lance and Williams, 1966, Emran and Ye, 2001), here
adapted to give the distance between the observation histogram H_o and the reference target histogram
H_t calculated on the same n bins:

175
$$d_{Canberra}(H_o, H_t) = \sum_{k=1}^{n} \left(\frac{|H_o(k) - H_t(k)|}{H_t(k)} \right)$$

where $H_i(k)$ is the value of histogram H_i at bin k. The smaller the Canberra distance, the more $H_o(p_i)$ and $H_t(p_i)$
are similar. To make the training dataset more representative of the parameter space in which the ANN will be
used, we assign to each observation and for a given parameter p_i, a weight $w_{obs}(p_i)$ equal to the ratio of $H_t(p_i)$ and
$H_o(p_i)$ for the bin where the observation is located. Consequently, if in a given bin, the observation histogram is
180 lower than the target histogram, meaning that this bin is underrepresented in the observational dataset compared
to the target space, then the weight $w_{obs}(p_i)$ will be greater than one and inversely. Eventually, for each
observation, we calculate the overall weight w_{obs} as the mean of $w_{obs}(p_1)$, $w_{obs}(p_2)$ and $w_{obs}(p_3)$. This overall weight
w_{obs} for each observation is used to calculate the loss function (in our case the mean squared error) minimized
during the training of the ANN. As a consequence, observations that are located in underrepresented regions of
185 the parameter space will have overall weights $w_{obs} > 1$ and will be given more importance in the training of the
ANN. Inversely, observations located in underrepresented parts of the parameter space will have overall weights
$w_{obs} < 1$ and will count less in the training of the ANN. The Canberra distance for $\overline{T_{2m,10\,y}}$, $\overline{SF_{10\,y}}$ and $T_{2m,\,amp}$
between observation and target histograms decreased from 22.6, 12.2 and 14.3 to 11.1, 7.5 and 5.3 when
weighing the observations based on their representativity (Figure 2). Another confirmation that the weights
190 increase the similarity between the observation and target histograms is the smaller difference between the
observation and target distributions' median values once the weights are applied: from 4.9 °C, 6.0 mm w.e., 2.4
°C with equal weights (Figure 2a-c) to 2.1 °C, 1.4 mm w.e. and 0.4 °C with weights (Figure 2d-f), for $\overline{T_{2m,10\,y}}$,
$\overline{SF_{10\,y}}$ and $T_{2m,\,amp}$ respectively.
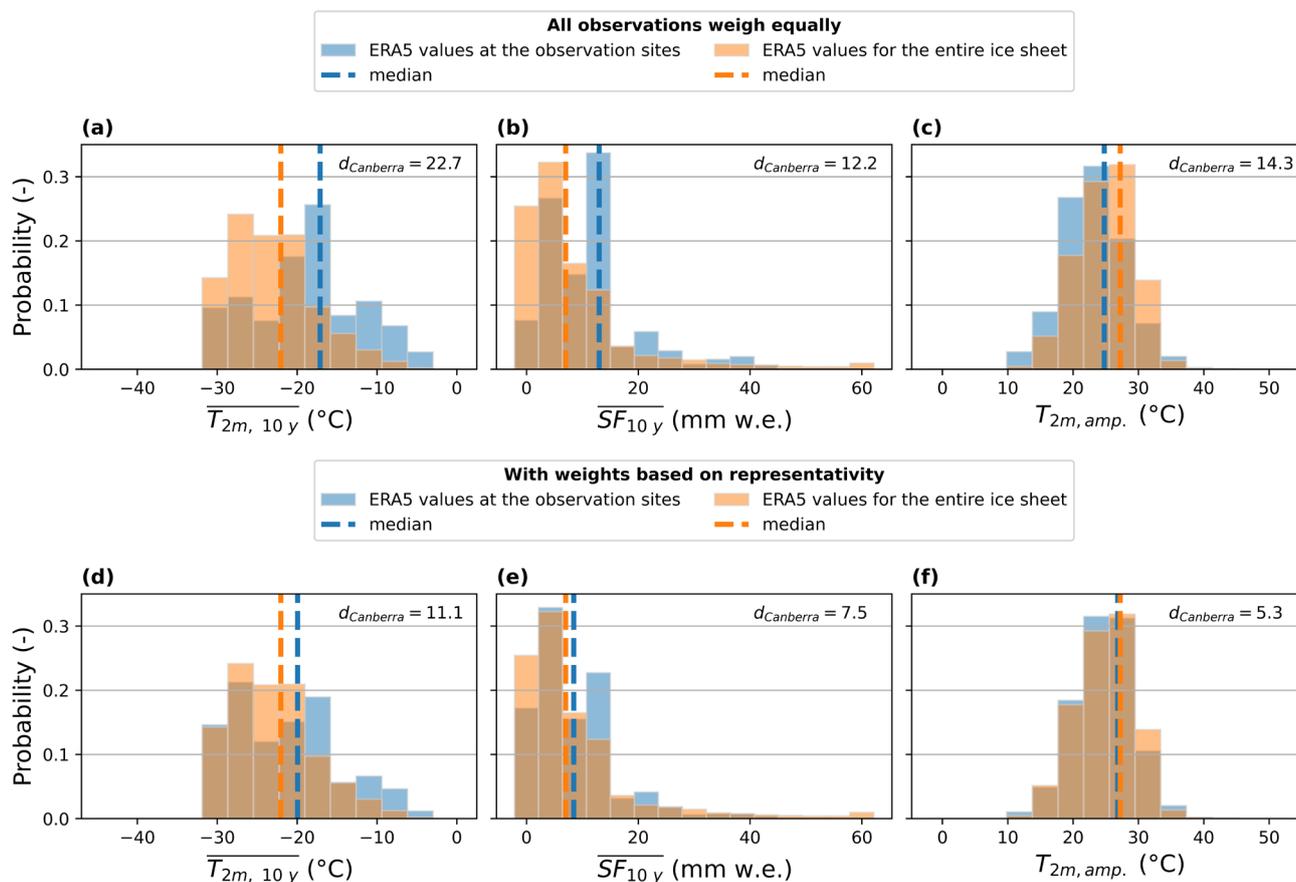
Figure 2: Histograms of the input parameters: 10 year average 2 m air temperature, 10 year average snowfall, annual amplitude of monthly 2 m air temperature. The blue histograms are parameter values as they appear at the observation sites, meaning the training data for the ANN, either with all observations weighing the same (a,b,c) or with weights assigned to each observation based on its representativity (d, e, f). The orange histograms are parameter values as they appear in the ice sheet pixels of ERA5, meaning the target data for the ANN. For each pair of target and observation histograms, we calculate the Canberra distance ($d_{Canberra}$) as a measure of similarity.

2.2.3. ANN structure and training

Multilayer perceptron ANNs are typically composed of an input layer, with as many nodes as input variables, multiple hidden layers containing several nodes, and an output layer. Each node in the hidden layers: i) makes the weighted sum of the outputs of all nodes from the preceding layer and adds a node-specific bias, ii) applies a simple, layer-specific activation function to the result, and ii) passes the output of the activation function to all the nodes of the next layer, and so forth. During the training of the model, all the weights and biases from all the nodes are being optimized to minimize a loss function. This is done iteratively by: i) passing part of the training

set through the ANN, ii) evaluating the difference between the ANN output and the expected result using the loss function, and iii) updating the weights and biases to reduce the error in the next iteration (a.k.a. backpropagation).

210   This general ANN structure can be adapted in many ways to the dataset and problem it is applied to. Here, we adjust four of the most important hyperparameters of the ANN: the batch size, i.e. which fraction of the sample is given to the ANN for every training cycle; the number of epochs (or training cycles); the number of layers and the numbers of nodes within those layers. We use the Adam optimizer (Kingma and Ba, 2014), rectified linear unit activation function (0 in input below 0, f(x)=x if input x above 0) and mean squared error as loss function.

215   Those three settings have been used widely in regression problems (Braakmann-Folgmann and Donlon, 2019; Liu et al., 2022, Lorentzen et al., 2022).

We set the hyperparameters of our ANN in three steps. First, we define a validation set made of 633 observations (14% of the training dataset) from four sites representing different areas of the ice sheet: NASA-E for the dry snow area,

220   NASA-SE for the percolation area and Swiss Camp and KAN_M for the bare ice area, and use these data as a validation set. Secondly, we train 1440 ANNs with two layers of 32 nodes each with batch sizes varying from 100 to 5000 (18 irregular steps) and between 10 and 1000 epochs (8 irregular steps), each the 144 settings are being run 10 times to account for the stochastic processes within model training. We assess the average learning curve for each setting: the mean difference (MD) and root mean squared difference (RMSD) of the

225   trained ANN on the training and validation data as a function of epoch numbers (Supplementary Figure 1). We conclude that: i) small batch sizes (<1000) lead to unstable learning curves (Supplementary Figure 1a-d) and ii) large batch sizes (e.g. 5000) cause slightly slower convergence and similar results as batch sizes of 3000 and 4000 (Supplementary Figure 1i-n). From our analysis and as a compromise between stability, rapidity of convergence and potential overfitting, we use a batch size of 4000 over 150 epochs for all ANN trained

230   henceforth. In the third and last step of our hyperparameter tuning, we use the optimal batch size and number of epochs to train 180 ANNs with either 1, 2 and 3 layers of 8, 16, 32, 64, 128 and 256 nodes each (all layers with same number of nodes, each setting repeated 10 times). We see clear improvements (lower RMSD) when moving from a single layer to two layers, and from 8 nodes to 64 nodes (Supplementary Figure 2). The improvement moving from 2 to 3 layers and from 64 to 128 or 256 nodes are marginal and within the stochastic uncertainty

235   (overlapping standard deviations in Supplementary Figure 2c-f). To keep the model design as simple as possible, we henceforth use two layers of 64 nodes each.

Additionally, a Gaussian noise layer that adds random noise to the observations is added after the input layer to
further prevent overfitting (e.g. An, 1996). Note that both the addition of Gaussian noise and the assignment of
240   weights to the observations will tend to decrease the apparent performance of the ANN (e.g. MD or RMSD from
the non-weighted observational dataset) but will produce a more robust output and prevent overfitting.
Considering the limited number of observations, we train our "best model" using all the available observations
weighted according to their representativity. In the absence of a hold out, or unseen data, we use a spatial cross-
validation approach to measure the performance and uncertainty of the ANN.

245   **2.2.4. Uncertainty estimation of the ANN with spatial cross-validation**

Spatial cross-validation is considered the best-practice approach for evaluating the uncertainty of ANN when
dealing with spatial data (e.g. Brenning et al., 2012). For this purpose, we separated the Greenland ice sheet into
10 regions (Figure 3c) after Zwally et al. (2012). Each of the 10 regions contain between 95 and 1298
observations, corresponding to 2% and 28% of all observations. For 10 iterations, we hold out the observations
250   located in a different region and train an ANN on the remaining observations. We save these 10 models and for
any new set of input parameters, we use the standard deviation of the 10 models' predictions as a measure of the
uncertainty. This uncertainty is never allowed to be below 0.5 $^{\circ}$C, which is the measurement uncertainty derived
in Section 2.1. The monthly grids of ANN uncertainty are provided along with our best estimation of T_{10m}, which
is produced by an ANN trained on all available observations.

255

For a fair evaluation of our ANN against our observational dataset, we first compare our best ANN model,
trained on all T_{10m} observations to these same T_{10m} observations. This evaluation does not show how the model
would perform on new, unseen data or regions, and consequently leads to an overestimation of the ANN
performance. We then compare each T_{10m} observation to the corresponding T_{10m} predicted by the one cross-
260   validation model that did not use this observation for training. This second evaluation illustrates how the cross-
validation ANNs perform on data that was not included in the training set. It contrasts with the first assessment,
because it evaluates models that were trained only on part of the observation dataset, and is therefore a
conservative estimate of the performance of the best model trained on all T_{10m} observations.

        2.3. Regional climate models

265   We evaluate 10 m subsurface temperatures from three regional climate models: MARv3.12 (Fettweis et al., 2017,
2020), RACMO2.3p2 (Noël et al., 2019) with the updated IMAU-FDMv1.2G (Brils et al., 2022) and HIRHAM5

(Langen et al., 2017). We calculate the MD and RMSD between the observed and simulated 10 m subsurface temperatures. For this study, the output from MAR, RACMO and HIRHAM are available over the periods 1950-2020, 1958-2020 and 1980-2016, respectively. We compare each model to the measurements within the common
270 1980-2016 period for which all three model outputs are available, as well as against all observations.

All three models use a multilayer snow, firn and ice model to calculate subsurface temperature. In addition to differences in surface forcing in the three models (e.g. in snowfall, rainfall, melt and energy fluxes), the models also differ in the way they calculate the subsurface characteristics that impact the subsurface temperature. Both MAR and HIRHAM estimate firn densification using the overburden pressure: respectively from Brun et al.
275 (1989) and Vionnet et al. (2012); while RACMO uses a compaction law that was derived for steady-state firn (Arthern et al., 2010) and empirically fitted to observations (Ligtenberg et al., 2011; Brils et al., 2022). RACMO's offline run with IMAU-FDMv1.2G uses the thermal conductivity parameterization from Calonne et al. (2019) while HIRHAM and MAR use the parameterization by Yen (1981). The three models treat the release of latent heat during the refreezing of meltwater in a similar manner, but the meltwater infiltration is calculated
280 differently. Both MAR and RACMO use a bucket scheme: meltwater infiltrates downward unless the water is refrozen or retained through capillary forces and ice layers are considered permeable at the model scale (Ligtenberg et al., 2018). HIRHAM, the use of a parameterization of Darcy flow (Hirashima et al., 2010) and accounting for the decrease of the layer permeability due to ice content (Colbeck, 1975), lead to shallower infiltration than in RACMO (Vandecrux et al., 2020b). Another model detail that impacts the calculated
285 subsurface temperature is the boundary condition at the bottom of the model domain. HIRHAM uses a temperature scheme that requires a fixed temperature at the lowermost firn layer which is set, for each pixel, to the long term air temperature average (Langen et al., 2017). Both MAR and RACMO use the Neumann boundary condition at the bottom layer of the firn model, which implies no heat flux through the lower boundary of the model. However, in the ablation area, new material needs to be provided to the bottom layer of the model as
290 surface ablation melts ice away. In MAR, as soon as the model column height is lower than 29 m, a 1 m thick layer composed of ice is added at the bottom of the model column. MAR then uses a simple assumption that the underlying ice would always be cooler than the ablating, near-surface ice. Consequently, the temperature of the 1 m layer added at the bottom of the model was fixed to be 1% lower (when calculated in Kelvin) than the temperature of the lowermost layer left in the model. The differences between RCM-simulated subsurface
295 temperatures are partly due to these different modeling approaches for the subsurface processes. This can be illustrated when different subsurface models are forced with similar surface data (Lundin et al., 2017; Vandecrux et al., 2020b). Another source of discrepancy is the difference in surface climate that is simulated in each of these

three models. More information about the accuracy of the simulated surface climate within each RCM can be found in Fettweis et al. (2020), Langen et al. (2017) and Noël et al. (2019).

3. Results

3.1. Performance of the ANN

When comparing the best ANN model to the T_{10m} observations it was trained on, we find a MD of 0.0°C and a RMSD of 1.6 °C (Figure 3a). However, when evaluating the cross-validation models against their respective unseen data, we find a similar MD (0.2°C) and a RMSD of 2.5 °C (Figure 3b). While the first evaluation is overoptimistic, the second does not evaluate directly our best ANN model, which is trained on all available data. These estimates nevertheless provide bounds to the true performance of our ANN. In both evaluations, the ANN fits almost equally well the ablation sites and dry snow sites (Figure 3a-b).

Averaging over the entire period 1950-2022, the ANN uncertainty is lowest across the dry snow area (Figure 3c), illustrated by the NASA-E site (Figure 3d). The uncertainty increases towards the ice sheet margin in west, north and northeast Greenland (Figure 3c) as exemplified by the sites DYE-2 in the percolation area in western Greenland (Figure 3e), KAN_L and KPC_U (Figure 3f-g), two ablation area sites in western and northeastern Greenland, respectively. The ANN uncertainty peaks in southeast Greenland (Figure 3c) where relatively high air temperatures and snow accumulation produce temperate firn conditions and firn aquifers (Forster et al., 2013; Kuipers Munneke et al., 2014). When the measurements in this region are removed for cross-validation, there is no firn aquifer observations left in the training set for the ANN to learn what the T_{10m} structure in this ice sheet region is, as illustrated in Figure 3h by a cross-validation model predicting lower T_{10m} than observed at the site FA_13. That results in a larger standard deviation between the cross-validation models for FA_13. Our uncertainty estimation is conservative because the final ANN model is eventually trained on all observations. The regions of high uncertainty highlight where observations are the most needed to map the ice sheet subsurface temperature.
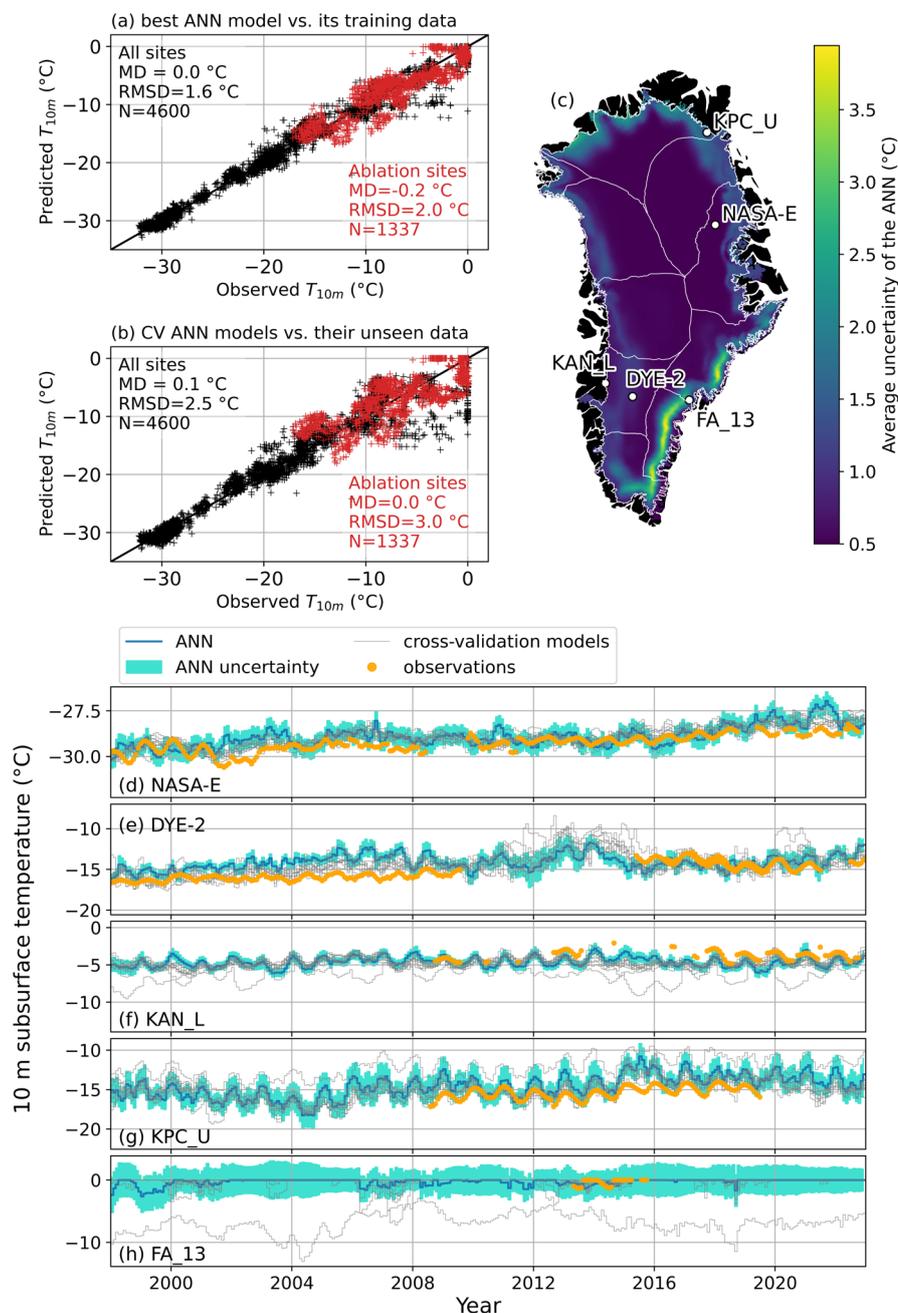
Figure 3. (a) Evaluation of the T_{10m} **simulated by the best ANN model against the observations used for training. (b) Evaluation of the** T_{10m} **simulated by the 10 cross-validation (CV) ANN models against their unseen data (i.e. not used for training). The statistics presented are mean difference (MD), root mean square difference (RMSD) and number of samples for which the comparison was possible (N). (c) 1950-2022 average of the ANN uncertainty as calculated from the standard deviation of 10 cross-validation ANN models trained on different spatial subsets of the observation dataset. (e-h) Examples of ANN** T_{10m} **prediction, its uncertainty and the prediction of the 10 cross-validation models at a dry snow site (NASA-E), one percolation site (DYE-2), two ablation sites (KAN_L, KPC_U), and a firn aquifer site (FA_13).**

3.2. RCM evaluation and comparison with the ANN

We evaluate the RCMs against the observed T_{10m} in the period 1980-2016 for which all three RCM's outputs are available (Figure 4). HIRHAM shows the best performance (MD = -0.4 ℃, RMSD = 2.8 ℃), followed by RACMO (MD = -1.3℃, RMSD = 3.1 ℃) and MAR (MD = +1.2 ℃, RMSD = 4.7 ℃). For the observation sites located in the ablation area, RACMO, HIRHAM and MAR have a cold bias with MD of -3.6, -0.9 and -3.4 ℃ respectively. MAR captures neither the geographical nor the seasonal variability of T_{10m} in the ablation area (RMSD = 5.4 ℃).
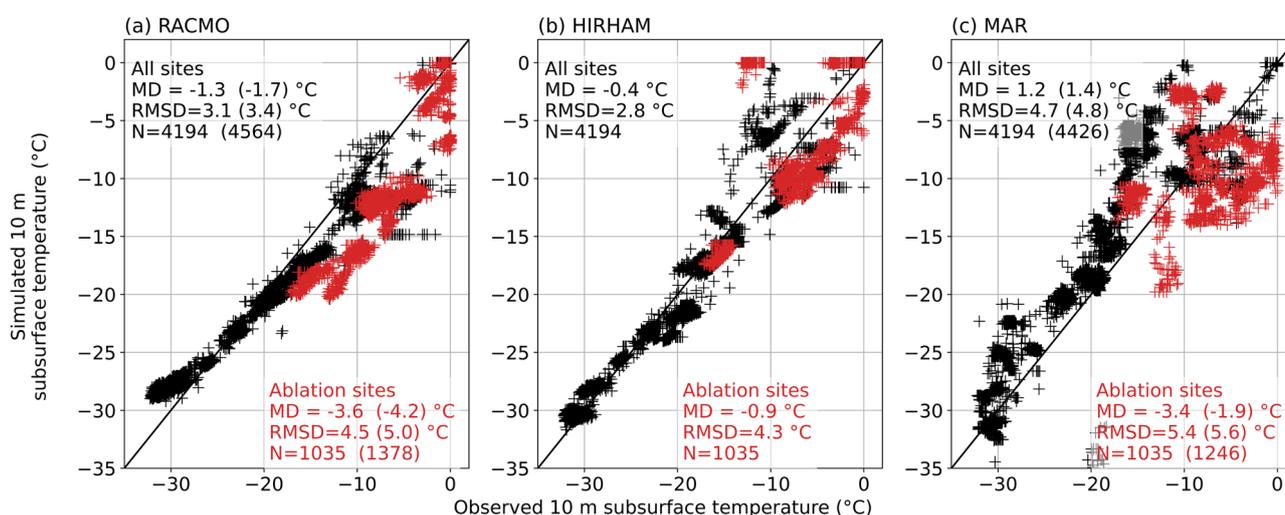
Figure 4. Evaluation of the monthly 10 m subsurface temperatures simulated by RACMO (a), HIRHAM (b) and MAR (c) against observations. The statistics presented are mean deviation (MD), root mean square difference (RMSD) and number of samples for which the comparison was possible (N) for the period when all three models are available (1980-2016). For RACMO and MAR, the statistics for all available measurements are given in the parenthesis. For sites where annual surface ablation is larger than snow accumulation, i.e., net ablation sites with a bare ice cover in summer, symbols and statistics are shown in red.

We further evaluate the ANN and RCMs at eight sites (Figure 5) that are representative of the dry snow (Summit, NASA-E), percolation (DYE-2, KAN_U), bare ice (Swiss Camp, KPC_U, SCO_U) and firn aquifer regions (FA_13). The ANN performs well at most of these sites: the average MD for these eight sites is less than 0.2℃ and the average RMSD is 1.2 ℃. RACMO overestimates T_{10m} at lower temperature sites in the dry snow area (Figure 5a-b) and underestimate T_{10m} at the accumulation sites with relatively high melt (Figure 5c-d) and at ablation sites (Figure 5e-g). HIRHAM compares better than RACMO to the measurements at accumulation sites (Figure 5a-b) and can either over- or underestimate T_{10m} at percolation sites (Figure 5c-d) and at ablation sites (Figure 5e-g). MAR simulates T_{10m} that are unrealistic both in magnitude and in variations (Figure 5). The causes of this low performance will be discussed in Section 4. At a firn aquifer site (Figure 5h) the ANN and the three

RCMs successfully estimate relatively high T_{10m} during the period 2013-2015 for which observations are available. Yet, the models diverge significantly when estimating the past history of the site: HIRHAM and MAR indicate T_{10m} close to 0 °C from the models' respective initiations in 1980 and 1950, while RACMO and the ANN indicate that T_{10m} below -2 °C may have been common at FA_13 before 2000 (Figure 5h).

355

Figure 5. Observed and simulated 10 m subsurface temperatures at selected sites. Note the different y-axis.

3.3. T_{10m} trends in the ANN and RCMs

According to the ANN, the Greenland ice sheet average T_{10m} has been increasing significantly at a rate of +0.2 °C decade^{-1} (P<0.01) over the 1950-2022 period (Table 2, Figure 6a), from an ice sheet-wide average value of -21.1 °C in 1950 to -19.2 °C in 2022. This increase was not constant over the 1950-2022 period. When fitting multiple piecewise linear functions to the Greenland ice sheet average T_{10m}, with breakpoint between 1951 and 2021, we identify 1985 as the breakpoint year that explains most of the variance in the ice-sheet-wide average T_{10m} time series. This piecewise linear function consists of a period of significant cooling between 1950 and 1985 (-0.4 °C decade^{-1}, P<0.01) followed by a strong warming from 1985 to 2022 (+0.7 °C decade^{-1}, P<0.01). Both cooling that occurred until 1985 and the subsequent warming were most pronounced in central and southern Greenland (Figure 7a-b). In contrast, the low elevations of the northwest Greenland ice sheet underwent warming during the entire period (Figure 7a–c).

For the time period for which ANN, RACMO, HIRHAM and MAR are available (1980-2016), the ANN gives an ice-sheet-wide average T_{10m} trend of 0.6 °C decade^{-1} (P<0.01) , while this warming is estimated at 0.3, 0.4, and -0.1 °C decade^{-1} by RACMO, HIRHAM and MAR (P≤0.01), respectively (Table 2, Figure 6a). The spatial patterns of T_{10m} trends in the three RCMs (Figure 7e-g) are consistent with the ANN (Figure 7d): a more pronounced warming at a mid-elevation band around the ice sheet and a milder warming (or cooling for MAR) in the rest of the ice sheet.

Since the processes controlling T_{10m} depend on the local climatic, snow and ice conditions, we also compare the evolution of T_{10m} in different ice sheet regions (Figure 1): the bare ice area where seasonal snow melts completely and exposes underlying glacial ice at the end of summer, the dry snow area where little or no melt occurs, and the intermediate percolation area where a significant portion of the annual snow accumulation melts in spring and summer and percolates into the underlying firn (Figure 1a). In the bare ice area (Figure 6b), the observation-based ANN predicts stable T_{10m} until the 1980s and increasing T_{10m} thereafter (+0.6 °C decade^{-1} over 1985-2022, P<0.01). In contrast, MAR estimates a negative trend in T_{10m} temperatures over the 1950-2022 period and overestimates the T_{10m} during the 1980-2000 period compared to the ANN (Figure 6b). In the bare ice area, RACMO and HIRHAM both present a T_{10m} trend of +0.2 °C decade^{-1} (P<0.01) over 1980-2016 period, which is 66% smaller than the ANN trend in the ablation area for the same period. In the dry snow area (Figure 6c), there is a better agreement between the models but lower T_{10m} in the 1990s in the ANN leads to a more pronounced

390 warming trend in that area (0.5 °C decade^{-1} over 1980-2016, P<0.01) which is 40-60 % larger than warming

trends predicted by RACMO and HIRHAM. MAR describes an overall cooling in the dry snow area (Figure 6c,

7g, Table 2). In the percolation area (Figure 6d), MAR has a warm bias compared to the other models (~+4 °C on

1980-2016), but all models agree on the strong warming that occurred since the 1980s: between 0.5 and 0.9 °C

decade^{-1} (all P<0.01) over 1980-2016 (Figure 6d, 7d-g, Table 2). Overall, these spatial differences average into a

395 warm bias of MAR for the entire ice sheet and more pronounced trends for the ANN than for the RCMs (Figure

6a).
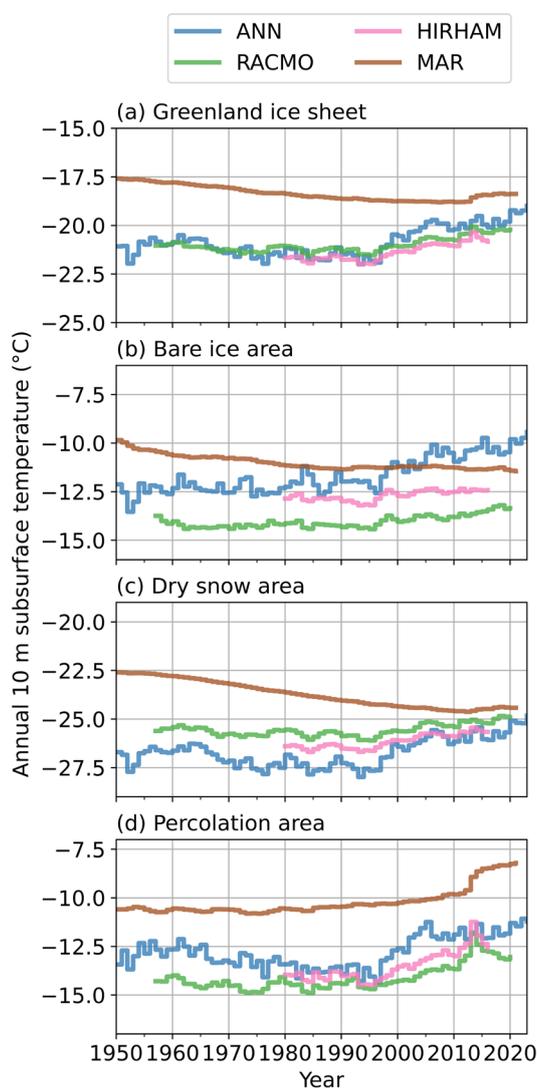
Figure 6. Evolution of the 10 m subsurface temperature (T$_{10m}$) for all of the Greenland ice sheet (a) and in three ice sheet regions (b-d). Although all panels have the same vertical axis scaling, note the different vertical axis bounds.
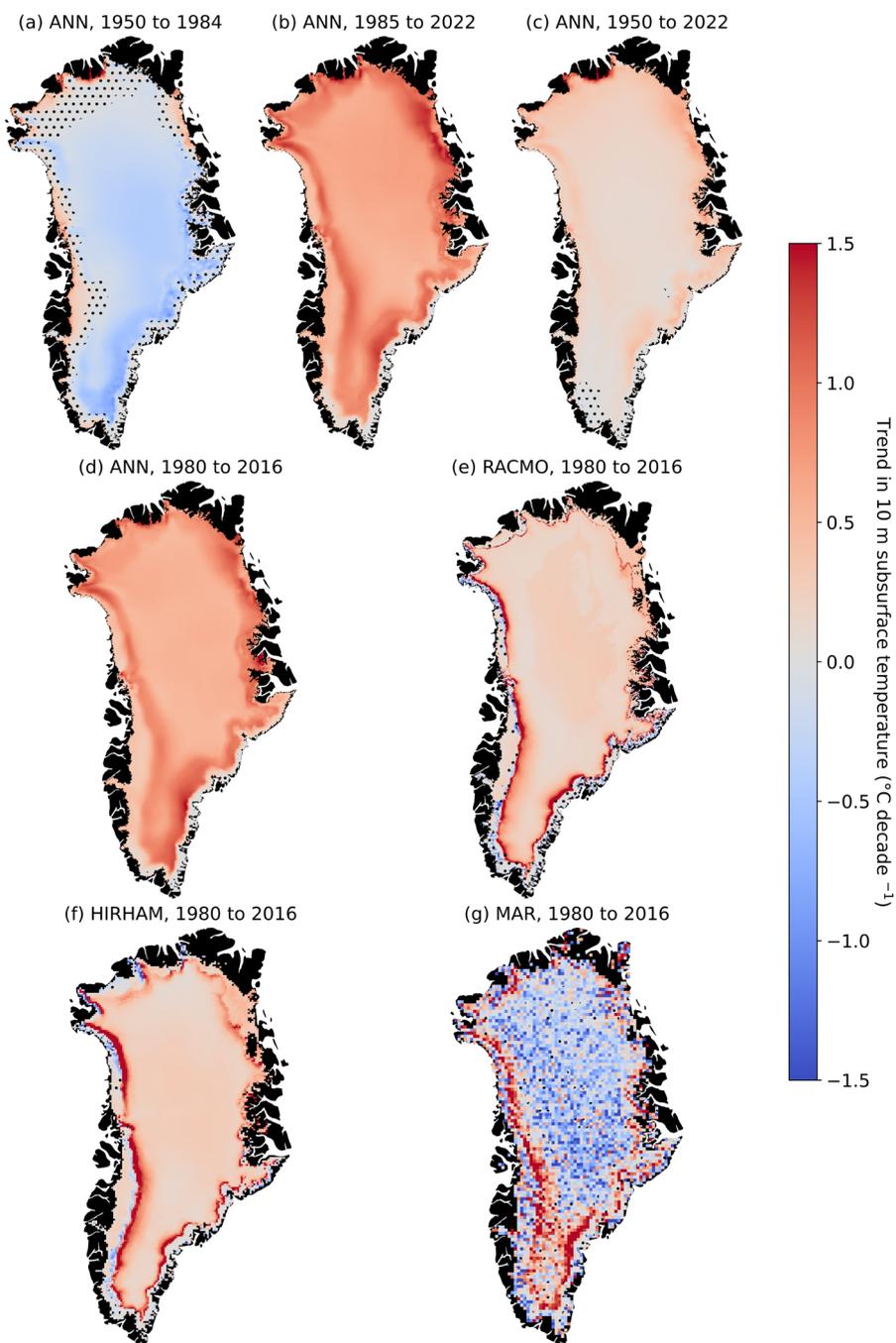
400

Figure 7. Trends in 10 m subsurface temperature as determined by the ANN over the periods 1950-1984 (a), 1985-2022 (b), 1950-2022 (c) and 1980-2016 (d), and calculated by RACMO (e), HIRHAM (f) and MAR (g) over the period 1980-2016, when data from all models are available. Dotted areas indicate trends below significance level (P > 0.1).

Table 2. Trends in 10 m subsurface temperature for different ice sheet regions and different periods. All trends are significant at a 0.1 level.

Model	Period	Mean T_{10m}	Trend in T_{10m} (°C decade^{-1})
All Greenland ice sheet			
ANN	1950-1985	-21.5	-0.4
ANN	1985-2022	-20.7	0.7
ANN	1950-2022	-21.1	0.2
ANN	1980-2016	-21.0	0.6
RACMO	1980-2016	-21.0	0.3
HIRHAM	1980-2016	-21.4	0.4
MAR	1980-2016	-18.6	-0.1
Bare ice area			
ANN	1950-1985	-10.8	0.1
ANN	1985-2022	-9.5	0.6
ANN	1950-2022	-10.1	0.4
ANN	1980-2016	-9.7	0.6
RACMO	1980-2016	-14.0	0.2
HIRHAM	1980-2016	-13.0	0.2
MAR	1980-2016	-11.3	-0.0
Dry snow area			
ANN	1950-1985	-27.1	-0.4
ANN	1985-2022	-26.5	0.6
ANN	1950-2022	-26.8	0.2
ANN	1980-2016	-26.8	0.5
RACMO	1980-2016	-25.6	0.2
HIRHAM	1980-2016	-26.1	0.3
MAR	1980-2016	-24.2	-0.3
Percolation area			
ANN	1950-1985	-13.5	-0.5
ANN	1985-2022	-12.8	0.9
ANN	1950-2022	-13.1	0.2
ANN	1980-2016	-13.1	0.8
RACMO	1980-2016	-14.0	0.6
HIRHAM	1980-2016	-13.5	0.6
MAR	1980-2016	-10.1	0.4

4. Discussion

We compiled the largest dataset of observed subsurface temperature to date and used it to train an ANN which,
410 with snowfall and temperature from ERA5 reanalysis as input, estimates monthly grids of 10 m subsurface
temperature over the entire ice sheet for the 1950-2022 period. The ANN describes a -0.4 $^{\circ}$C decade^{-1} T_{10m}
decrease during 1950-1985 (Figure 6a, Table 2) which is consistent with the negative trends in air temperatures
found by Zhang et al. (2022) in the ERA5 reanalysis and RACMO RCM from the late 1950s to early 1990s. The
following increase in T_{10m} calculated by the ANN from the 1990s to 2022 is consistent with all-year and summer
415 air temperature increases found in weather station observations, reanalysis datasets and regional climate models
(Hanna et al., 2021, Zhang et al., 2022). The ice sheet wide average T_{10m} trend, +0.2 $^{\circ}$C decade^{-1} over 1950-2022,
agrees with the trend in annual air temperature in ERA5 (+0.2 $^{\circ}$C decade^{-1} over 1950-2022). Additionally, the
ANN estimates a strong warming (+0.9 $^{\circ}$C decade^{-1}) in the upper percolation area during the 1985-2022 period
(Figure 6d, 7b, Table 2). This localized warming of the percolation area is also calculated by the three RCMs
420 (Figure 6d, Figure 7e-g). However, this hotspot of T_{10m} increase is not found in air temperature trends (Zhang et
al., 2022 Fig. 5-7). The warming of the subsurface in the percolation area stems from the increased meltwater
infiltration and from the latent heat released by refreezing (e.g. Humphrey et al., 2012; Vandecrux et al., 2020a).
This successful identification of areas subject to firn warming by the ANN is remarkable considering that the
ANN only learns from the T_{10m} observations, and the local air temperature and snowfall history, and is not fed
425 information on meltwater infiltration and refreezing. This indicates that the ANN successfully learns from the
data which areas are susceptible to undergo meltwater infiltration and refreezing.

The ANN model has the strength of statistical models: it fits the training data and thereby performs better than
RCMs when evaluated against observations used for training (Figure 3a, 4). Yet, ANN and statistical models
430 have several limitations. Firstly, the ANN is greatly dependent on the distribution of the training data, and how
representative that data is of the parameter space where the ANN is applied. Our methods give more weight to
observations that are from underrepresented areas of the parameter space. Yet, there are still regions with
particular combinations of air temperature and snowfall where no observations are available and where the ANN
extrapolates. More observations are needed from these less-visited parts of the ice sheet to further train the ANN.
435 Secondly, the ANN is limited by the input parameters it draws on. For instance, inaccuracies in ERA5 data (as

discussed in Delhasse et al., 2020; Zhang et al., 2022) for certain periods or locations will affect the performance of the ANN, as will T_{10m} measurement uncertainties. Besides, only using two input parameters (air temperature and snowfall) must introduce inaccuracy through oversimplification of complex physical processes. Additionally, the relatively coarse resolution of the input grid (0.1x0.1°) prevents the ANN from identifying local phenomena

440   such as localized meltwater refreezing in surface deepenings and crevasses (Hills et al., 2018, Chudley et al., 2021) or in ephemeral perched aquifers (Humphrey et al., 2021, Culberg et al., 2022). Neither can our ANN model account for the exposure of ice affected by past temperature anomalies, i.e. the advection of deep ice in the ablation zone that may drive T_{10m} more than surface conditions (Lüthi et al., 2015). Other widespread processes such as the penetration of short-wave radiation into the subsurface (Van den Broeke et al., 2008; Kuipers

445   Munneke et al., 2009; Van Dalum et al., 2021), firn ventilation (Albert and Shultz, 2002) or potentially 'wind pumping' (Clarke et al., 1987) are more likely to be accounted for by the ANN because observations subject to these processes are included in the dataset. Ultimately, the ANN cannot identify the processes that are responsible for a given subsurface temperature, but it can learn which T_{10m} are usually seen at various temperature and snowfall combinations.

450

Although the RCMs calculate subsurface temperatures in similar ways (see Section 2.3), differences arise due to their various assumptions. For example, MAR assumes that in the ablation area, the material added at the lower bound of the model column is always slightly colder than the lowermost material left in the column. This explains the decreasing trend in simulated T_{10m} in Figure 6a and the inability of MAR to explain the observed

455   T_{10m} variation at the ablation sites (Figure 4c). The noise within the T_{10m} trend map (Figure 7g) is also indicative of some numerical instability in this deep temperature prescription. These limitations of the model's boundary conditions have now been identified and efforts are ongoing to remediate them in the next version of MAR. It is, however, interesting to note that these biases do not significantly impact the surface mass balance simulated by MAR; different sensitivity tests were performed with the aim of improving the comparison with T_{10m} and for all

460   of them, the MAR results at the surface remained unchanged. Langen et al. (2017) showed that the simulated subsurface temperature profile in HIRHAM in the percolation area greatly depends on the formation, in the model, of ice layers of density greater than 830 kg m^{-3} that inhibit water infiltration. The formation of these high density layers in the model depends on the surface climate and subsurface model, but also on the discretization of the modeled firn column, which is currently fixed in HIRHAM (Vandecrux et al., 2020b). Recent efforts to

465   update the HIRHAM subsurface scheme to a more flexible discretization that would preserve high density layers was made for Antarctica (Hansen et al. 2021) but has not yet been applied to Greenland. Steger et al. (2017)

found that the SNOWPACK model forced by RACMO2.3, an older version of RACMO2.3p2 evaluated here, overestimated the subsurface temperature in the high elevation areas in northwestern Greenland, while underestimating the firn temperature at lower elevations due to either insufficient meltwater generation at the surface or too shallow simulated meltwater infiltration. In that same study, RACMO2.3 in combination with both IMAU-FDMv1.1 and SNOWPACK subsurface schemes could not accurately reproduce subsurface temperatures at some low percolation sites because the models represented them as bare ice sites. This mismatch between the simulated and actual surface type – bare ice or porous firn – makes sites at the transition between the bare ice and percolation areas, i.e., the equilibrium line, particularly challenging for all RCMs (e.g., KAN_U, Swiss Camp, KPC_U in Figure 5d-f). Switching from version 2.3 to 2.3p2, in combination with an update to IMAU-FDMv1.2 allowed RACMO to simulate KAN_U as a firn site rather than a bare ice site (Ligtenberg et al., 2018, Brils et al., 2022). The IMAU-FDM always allows meltwater infiltration, which may lead to an overestimation of T_{10m} at sites where thick ice layers in the firn provide a barrier for further percolation. This was highlighted at KAN_U when driving IMAU-FDMv1.1 with surface temperature and melt rates derived from observations (Vandecrux et al., 2020b). However, the updated IMAU-FDMv1.2 forced by RACMO2.3p2 now shows a slight cold bias at KAN_U (Figure 5d), indicating that too deep meltwater infiltration is no longer an issue at that site (Brils et al., 2022).

The subsurface temperature impacts the surface energy budget through the conductive heat flux, and thereby affects the snow and ice surface melt. Heat from a warm subsurface will be conducted to the surface when surface temperatures are lower. And vice-versa, a colder subsurface represents a heat sink (heat will conduct down, away from the surface) and will moderate surface melt. Another consequence of the near-surface snow and firn warming is that it decreases the cold content and therefore the retention capacity of the snow and firn (Pfeffer et al., 1991; Vandecrux et al., 2020a). Meltwater retention in firn occurs when 1) pore space is available, 2) this pore space can be accessed by the meltwater and 3) cold content is available to refreeze the meltwater. Vandecrux et al. (2019) documented that the upper 10 m of the firn in the lower accumulation and percolation area lost about 20% of its pore space over the last decades, while in the dry snow area pore space remained stable since the 1950s. Our work documents the recent subsurface warming of the ice sheet and how the upper 10 m of snow, ice and firn is brought closer to the melting point, potentially enhancing meltwater runoff in the subsequent summers. For instance, the dry snow area average T_{10m} increased from -27.3 ºC over 1980-1990 to -25.8 ºC over 2010-2020. The percolation area warmed from -13.7 ºC over 1980-1990 to -11.8 ºC over 2010-2020; 1.9 ºC (14%) closer to the melting point. Our findings complement other work showing the changes in the Greenland ice

sheet subsurface their impact on the ice sheet mass loss: for example the recent expansion of the firn aquifer area stemming, among other causes, from the loss of firn cold content (Horlings et al., 2022) or the increasing the

500 runoff from the firn area (Tedstone and Machguth, 2022) linked to the formation of ice layers reducing meltwater percolation and retention into the underlying firn (Machguth et al., 2016; MacFerrin et al., 2019) .

5. Conclusion

Using the most complete compilation of observed T_{10m} on the Greenland ice sheet to date, we trained an Artificial Neural Network (ANN) to describe the spatio-temporal evolution of T_{10m} during 1950-2022. We found that,

505 following a significant cooling between 1950 and 1985 (-0.4 °C decade^{-1}, P<0.1), ice sheet-wide T_{10m} increased by +0.7 °C decade^{-1} from 1985 to 2022 (P<0.1). Overall, the Greenland ice sheet T_{10m} increased at a rate of +0.2 °C decade^{-1} over the 1950-2022 period in response to increasing energy influx at the surface. Our observational dataset yielded unique and extensive constraints on the subsurface temperature simulated by three conventional regional climate models, RACMO, MAR and HIRHAM and demonstrated their mixed performance. Notably, it

510 revealed numerical instabilities in MAR prompting improvements in its snow module, although these T_{10m} biases apparently have low impact on the SMB simulated by MAR. This work highlights the value of in-situ measurements of ice, snow and firn temperatures to better quantify the response of the Greenland ice sheet to Arctic warming and to reduce uncertainty in projections of mass loss from the Greenland ice sheet.

6. Data and code availability

515 The original subsurface temperature datasets are cited in Table 1 and, when available, download links to the original datasets can be found in the reference list. Some of the observational data was found in other compilations such as Mock and Weeks (1965), McGrath et al. (2013) or Løkkegaard et al. (2022) and Mankoff et al. (2022).

520 The monthly T_{10m} dataset is currently hosted at https://doi.org/10.22008/FK2/TURMGZ (Vandecrux, 2023a) and will be added to the next release of the SUMup dataset (Thompson-Munson et al., 2022). A compilation of non-interpolated, instantaneous subsurface temperatures can be requested from the authors. The T_{10m} maps here are available at https://doi.org/10.22008/FK2/C24WVN (Vandecrux, 2023b) and the scripts used for the analysis are available at https://doi.org/10.5281/zenodo.8027442 (Vandecrux, 2023c).

7. Acknowledgments

BV designed the study, processed and compiled the observations, and conducted the analysis with the help from RSF, JEB, FC, RH, AKR. RSF. RSF, APA, JEB, FC, RH, AKR, AH, JA, PCJPS and DvA funded or organized projects measuring subsurface temperatures and provided valuable data. EB provided insights in the ANN setup and tuning. XF, PKM, MRvdB, MB, PLL, RM provided RCM outputs and insights on their performance. BV drafted the manuscript, to which all co-authors contributed.

8. Competing interests

XF, RM and MRvdB. are members of the editorial board of the Cryosphere.

9. Acknowledgments

We salute the field parties that collected data in the field over more than 100 years, allowing us to conduct the present analysis. The PROMICE and the new GC-Net AWS are supported by the Danish Ministry for Environment, Energy and Utilities. The historical GC-Net AWS and FirnCover were supported by NASA, NSF and WSL grants. JA was supported by the Austrian Science Fund (P35388). F. Covi, Å. Rennermalm and R. Hock were supported by NSF grant no. 397516-66782. We also thank Hubertus Fischer, Wilfried Häberli, Olaf Eisen, Shin Sugiyama, Sumito Matoba and Robert Hawley for sharing their subsurface temperature data. MRvdB, PKM and MB acknowledge funding from the Netherlands Earth System Science Centre (NESSC). PLL gratefully acknowledges funding from the Aarhus University Interdisciplinary Centre for Climate Change (iClimate, Aarhus University). AH has been supported by the DFG (Deutsche Forschungsgemeinschaft; grant no. HE7501/1-1).

References

Abermann, J., Vandecrux, B., Scher, S., Löffler, K., Schalamon, F., Trügler, A., Fausto, R.S., Schöner, W.:. Learning from Alfred Wegener's pioneering field observations in West Greenland after a century of climate change. *Sci Rep* **13**, 7583, https://doi.org/10.1038/s41598-023-33225-9, 2023.

Ahlstrøm, A. P. ., and the PROMICE project team:. A new programme for monitoring the mass loss of the Greenland ice sheet. *GEUS Bulletin*, *15*, 61–64. https://doi.org/10.34194/geusb.v15.5045, 2008.

Albert, M. R. and Shultz, E. F.: Snow and firn properties and air–snow transport processes at Summit, Greenland, Atmos. Environ., 36(15–16), 2789–2797, https://doi.org/10.1016/S1352-2310(02)00119-X, 2002.

Ambach, W., Zum Wärmehaushalt des Grönländischen Inlandeises: Vergleichende Studie im Akkumulations- und Ablationsgebiet, Polarforschung 49 (1): 44-54, 1979

Arthern, R. J., Vaughan, D. G., Rankin, A. M., Mulvaney, R., and Thomas, E. R.: In situ measurements of Antarctic
555   snow compaction compared with predictions of models, J. Geophys. Res.-Earth Surf., 115, 1–12, https://doi.org/10.1029/2009JF001306, 2010.

Benson, C. S.: Stratigraphic Studies in the Snow and Firn of the Greenland ice sheet. Research Report 70. Reprinted August 1996 with revision of Cold Regions Research Laboratory (CRRL), , (August), 93 [online] Available from: http://acwc.sdp.sirsi.net/client/search/asset/1001392, 1962.

560   Bjerre, E., Fienen, M.N., Schneider, R., Koch, J. and Højberg, A.L.: Assessing spatial transferability of a random forest metamodel for predicting drainage fraction. *Journal of Hydrology*, *612*, p.128177, https://doi.org/10.1016/j.jhydrol.2022.128177, 2022.

Box, J. E., Fettweis, X., Stroeve, J. C., Tedesco, M., Hall, D. K., and Steffen, K.: Greenland ice sheet albedo feedback: thermodynamics and atmospheric drivers, The Cryosphere, 6, 821–839, https://doi.org/10.5194/tc-6-821-2012, 2012.

565   Braakmann-Folgmann, A. and Donlon, C.: Estimating snow depth on Arctic sea ice using satellite microwave radiometry and a neural network, The Cryosphere, 13, 2421–2438, https://doi.org/10.5194/tc-13-2421-2019, 2019.

Braithwaite, R.:. Firn temperature and meltwater refreezing in the lower accumulation area of the Greenland ice sheet, Pâkitsoq, West Greenland. Rapport Grønlands Geologiske Undersøgelse, 159, 109–114. https://doi.org/10.34194/rapggu.v159.8218, 1993.

570   Brenning, A., "Spatial cross-validation and bootstrap for the assessment of prediction rules in remote sensing: The R package sperrorest," *2012 IEEE International Geoscience and Remote Sensing Symposium*, Munich, Germany, pp. 5372-5375, https://doi.org/10.1109/IGARSS.2012.6352393, 2012.

Brils, M., Kuipers Munneke, P., van de Berg, W. J., and van den Broeke, M.: Improved representation of the contemporary Greenland ice sheet firn layer by IMAU-FDM v1.2G, Geosci. Model Dev., 15, 7121–7138,
575   https://doi.org/10.5194/gmd-15-7121-2022, 2022.

Brun, E., Martin, E., Simon, V., Gendre, C. and Coleou, C.: An energy and mass model of snow cover suitable for operational avalanche forecasting. *Journal of glaciology*, *35*(121), pp.333-342, https://doi.org/10.3189/S0022143000009254, 1989.

Calonne, N., Milliancourt, L., Burr, A., Philip, A., Martin, C. L., Flin, F., and Geindreau, C.:. Thermal conductivity of
580   snow, firn, and porous ice from 3-D image-based computations. Geophys. Res. Lett., 46, 13079–13089, https://doi.org/10.1029/2019GL085228, 2019.

Charalampidis, C., Van As, D., Colgan, W. T., Fausto, R. S., Macferrin, M. and Machguth, H.: Thermal tracing of retained meltwater in the lower accumulation area of the Southwestern Greenland ice sheet, Ann. Glaciol., 57(72), 1–10, https://doi.org/10.1017/aog.2016.2, 2016.

585 Charalampidis, C., van As, D., Colgan, W., Fausto, R., MacFerrin, M., Machguth, H., Vandecrux, B.: Subsurface monitoring at 1840 m a.s.l. on the southwestern Greenland ice sheet during 2012–2013, GEUS Dataverse, https://doi.org/10.22008/FK2/OVGQZ9, 2022.

Chudley, T. R., Christoffersen, P., Doyle, S. H., Dowling, T. P. F., Law, R., Schoonman, C. M., M. Bougamont, B. Hubbard: Controls on water storage and drainage in crevasses on the Greenland Ice Sheet. *Journal of Geophysical Research:*
590 *Earth Surface*, 126, e2021JF006287. https://doi.org/10.1029/2021JF006287, 2021.

Chylek, P., Folland, C., Klett, J. D., Wang, M., Hengartner, N., Lesins, G., and Dubey, M. K.: Annual mean Arctic Amplification 1970–2020: Observed and simulated by CMIP6 climate models. *Geophysical Research Letters*, 49, e2022GL099371. https://doi.org/10.1029/2022GL099371, 2022.

Clarke, G. K. C., Fisher, D. A. and Waddington, E. D.: Wind pumping: A potentially significant heat source in ice sheets,
595 Phys. Basis Ice Sheet Model. IAHS Publ., (170), 169–180, 1987.

Clausen, H. B. and Hammer, C. U.: The Laki and Tambora Eruptions as Revealed in Greenland Ice Cores from 11 Locations, Ann. Glaciol., 10, 16–22, https://doi.org/10.1017/s0260305500004092, 1988.

Clausen, H. B., Gundestrup, N. S., Johnsen, S. J., Bindschadler, R. A. and Zwally, J.: Glaciological investigations in the Crête area, central Greenland: a search for a new deep-drilling site, Ann. Glaciol., 10, 10–15, 1988.

600 Clement, P.: Glaciological Activities in the Johan Dahl Land Area, South Greenland, As a Basis for Mapping Hydropower Potential. Rapport Grønlands Geologiske Undersøgelse, vol. 120, pp. 113-21, https://doi.org/10.34194/rapggu.v120.7870, 1984.

Colbeck, S. C.: A theory for water flow through a layered snowpack, Water Resour. Res., 11, 261–266, https://doi.org/10.1029/WR011i002p00261, 1975.

605 Colbeck, S. C. and Gow, A. J.: The Margin of the Greenland ice sheet at Isua, J. Glaciol., 24(90), 155–165, https://doi.org/10.3189/s0022143000014714, 1979.

Colgan, W., Sommers, A., Rajaram, H., Abdalati, W. and Frahm, J.: Considering thermal-viscous collapse of the Greenland ice sheet. Earth's Future, 3: 252-267. https://doi.org/10.1002/2015EF000301, 2015.

Colgan, W.; Vandecrux, B.: Camp Century: Firn temperature measurements (CEN-THM), GEUS DAtaverse,
610 https://doi.org/10.22008/FK2/SR3O4F, 2021.

Cook, J. M., Tedstone, A. J., Williamson, C., McCutcheon, J., Hodson, A. J., Dayal, A., Skiles, M., Hofer, S., Bryant, R., McAree, O., McGonigle, A., Ryan, J., Anesio, A. M., Irvine-Fynn, T. D. L., Hubbard, A., Hanna, E., Flanner, M., Mayanna, S., Benning, L. G., Van As, D., Yallop, M., McQuaid, J. B., Gribbin, T. and Tranter, M.: Glacier algae accelerate melt rates on the south-western Greenland ice sheet, The Cryosphere, 14(1), 309–330, https://doi.org/10.5194/tc-14-309-2020, 2020.

615 Covi, F., Hock, R., Rennermalm, A., Leidman, S., Miege, C., Kingslake, J., Xiao, J., MacFerrin, M., Tedesco, M.:. Meteorological and firn temperature data from three weather stations in the percolation zone of southwest Greenland, 2017 - 2019. Arctic Data Center, https://doi.org/10.18739/A2BN9X444, 2022.

Covi, F., Hock, R., and Reijmer, C.: Challenges in modeling the energy balance and melt in the percolation zone of the Greenland ice sheet. *Journal of Glaciology, 69*(273), 164-178. https://doi.org/10.1017/jog.2022.54, 2023.

620 Cuffey, K. M. and Paterson, W. S. B.: The physics of glaciers, 4th Edition. [online] Available from: https://www.elsevier.com/books/the-physics-of-glaciers/cuffey/978-0-12-369461-4 (Accessed 25 November 2021), 2010.

Culberg, R., Chu, W., & Schroeder, D. M.: Shallow fracture buffers high elevation runoff in Northwest Greenland. *Geophysical Research Letters*, 49, e2022GL101151. https://doi.org/10.1029/2022GL101151, 2022.

Dahl-Jensen, D., Mosegaard, K., Gundestrup, N., Clow, G. D., Johnsen, S. J., Hansen, A. W. and Balling, N.: Past
625 temperatures directly from the Greenland ice sheet, Science (80-.)., 282(5387), 268–271, https://doi.org/10.1126/science.282.5387.268, 1998.

Davis, T.C., Structures in the upper snow layers of the southern Dome Greenland ice sheet, CRREL research report 115, https://hdl.handle.net/11681/5839, 1954

Davis R.M.: Approach roads Greenland 1960-1964 Technical Report 133. Corps of Engineers Cold Regions Research
630 and Engineering Laboratory, https://hdl.handle.net/11681/5708, 1967.

Delhasse, A., Kittel, C., Amory, C., Hofer, S., van As, D., S. Fausto, R., and Fettweis, X.: Brief communication: Evaluation of the near-surface climate in ERA5 over the Greenland Ice Sheet, The Cryosphere, 14, 957–965, https://doi.org/10.5194/tc-14-957-2020, 2020.

Echelmeyer, K., Harrison, W. D., Clarke, T. S. and Benson, C.: Surficial glaciology of Jakobshavns Isbrae, west
635 Greenland: part II. Ablation, accumulation and temperature, J. Glaciol., 38(128), 169–181, https://doi.org/10.1017/S0022143000009709, 1992.

Emran, S.M. and Ye, N.: Robustness of canberra metric in computer intrusion detection. In Proc. IEEE Workshop on Information Assurance and Security, West Point, NY, USA (pp. 80-84), URL, 2001.

Fausto, R. S., van As, D., Mankoff, K. D., Vandecrux, B., Citterio, M., Ahlstrøm, A. P., Andersen, S. B., Colgan, W.,
640 Karlsson, N. B., Kjeldsen, K. K., Korsgaard, N. J., Larsen, S. H., Nielsen, S., Pedersen, A. Ø., Shields, C. L., Solgaard, A. M., and Box, J. E.: Programme for Monitoring of the Greenland Ice Sheet (PROMICE) automatic weather station data, Earth Syst. Sci. Data, 13, 3819–3845, https://doi.org/10.5194/essd-13-3819-2021 , 2021.

Fausto, R., van As, D., and Mankoff, K. D.: Programme for monitoring of the Greenland ice sheet (PROMICE): Automatic weather station data, Version: v03 [data set], Geological survey of Denmark and Greenland (GEUS),
645 https://doi.org/10.22008/promice/data/aws, 2019.

Fettweis, X., Box, J. E., Agosta, C., Amory, C., Kittel, C., Lang, C., Van As, D., Machguth, H. and Gallée, H.: Reconstructions of the 1900-2015 Greenland ice sheet surface mass balance using the regional climate MAR model, The Cryosphere, 11(2), 1015–1033, https://doi.org/10.5194/tc-11-1015-2017, 2017.

Fettweis, X., Hofer, S., Krebs-Kanzow, U., Amory, C., Aoki, T., Berends, C. J., Born, A., Box, J. E., Delhasse, A.,
650 Fujita, K., Gierz, P., Goelzer, H., Hanna, E., Hashimoto, A., Huybrechts, P., Kapsch, M.-L., King, M. D., Kittel, C., Lang, C., Langen, P. L., Lenaerts, J. T. M., Liston, G. E., Lohmann, G., Mernild, S. H., Mikolajewicz, U., Modali, K., Mottram, R.

H., Niwano, M., Noël, B., Ryan, J. C., Smith, A., Streffing, J., Tedesco, M., van de Berg, W. J., van den Broeke, M., van de Wal, R. S. W., van Kampenhout, L., Wilton, D., Wouters, B., Ziemen, F., and Zolles, T.: GrSMBMIP: intercomparison of the modelled 1980–2012 surface mass balance over the Greenland Ice Sheet, The Cryosphere, 14, 3935–3958, https://doi.org/10.5194/tc-14-3935-2020, 2020.

Forster, R. R., Box, J. E., van den Broeke, M. R., Miège, C., Burgess, E. W., van Angelen, J. H., Lenaerts, J. T. M., Koenig, L. S., Paden, J., Lewis, C., Gogineni, S. P., Leuschen, C., and McConnell, J. R.: Extensive liquid melt water storage in firn within the Greenland ice sheet, Nat. Geosci., 7, 95–98, https://doi.org/10.1038/NGEO2043, 2013

Giese, A. L. and Hawley, R. L.: Reconstructing thermal properties of firn at Summit, Greenland, from a temperature profile time series, J. Glaciol., 61(227), 503–510, https://doi.org/10.3189/2015JoG14J204, 2015.

Griffiths, T. M. (1960). Glaciological investigations in the TUTO area of Greenland., U. S. Army Snow Ice and Permafrost Research Establishment, Corps of Engineers, Report 47, 62 pp.

Hanna, E., Cappelen, J., Fettweis, X., Mernild, S. H., Mote, T. L., Mottram, R., Steffen, K., Ballinger, T. J. and Hall, R. J.: Greenland surface air temperature changes from 1981 to 2019 and implications for ice-sheet melt and mass-balance change, Int. J. Climatol., 41(S1), E1336–E1352, https://doi.org/10.1002/joc.6771, 2021.

Hansen, N., Langen, P. L., Boberg, F., Forsberg, R., Simonsen, S. B., Thejll, P., Vandecrux, B., and Mottram, R.: Downscaled surface mass balance in Antarctica: impacts of subsurface processes and large-scale atmospheric circulation, The Cryosphere, 15, 4315–4333, https://doi.org/10.5194/tc-15-4315-2021, 2021.

Harrington, J. A., Humphrey, N. F. and Harper, J. T.: Temperature distribution and thermal anomalies along a flowline of the Greenland ice sheet, Ann. Glaciol., 56(70), 98–104, https://doi.org/10.3189/2015AoG70A945, 2015.

Heilig, A., Eisen, O., MacFerrin, M., Tedesco, M., and Fettweis, X.: Seasonal monitoring of melt and accumulation within the deep percolation zone of the Greenland ice sheet and comparison with simulations of regional climate modeling, The Cryosphere, 12, 1851–1866, https://doi.org/10.5194/tc-12-1851-2018, 2018.

Hersbach, H., Bell, B., Berrisford, P., Hirahara, S., Horányi, A., Muñoz-Sabater, J., Nicolas, J., Peubey, C., Radu, R., Schepers, D., Simmons, A., Soci, C., Abdalla, S., Abellan, X., Balsamo, G., Bechtold, P., Biavati, G., Bidlot, J., Bonavita, M., Chiara, G., Dahlgren, P., Dee, D., Diamantakis, M., Dragani, R., Flemming, J., Forbes, R., Fuentes, M., Geer, A., Haimberger, L., Healy, S., Hogan, R. J., Hólm, E., Janisková, M., Keeley, S., Laloyaux, P., Lopez, P., Lupu, C., Radnoti, G., Rosnay, P., Rozum, I., Vamborg, F., Villaume, S., and Thépaut, J.: The ERA5 global reanalysis, Q. J. Roy. Meteor. Soc., 146, 1999–2049, https://doi.org/10.1002/qj.3803, 2020.

Hersbach, H., Bell, B., Berrisford, P., Biavati, G., Horányi, A., Muñoz Sabater, J., Nicolas, J., Peubey, C., Radu, R., Rozum, I., Schepers, D., Simmons, A., Soci, C., Dee, D., Thépaut, J-N.: ERA5 monthly averaged data on single levels from 1940 to present. Copernicus Climate Change Service (C3S) Climate Data Store (CDS), https://doi.org/10.24381/cds.f17050d7, 2023.

Heuberger, J.-C.: Volume 1: Forages sur l'inlandsis, in Expéditions Polaires Françaises: Missions Paul-Émile Victor. Glaciologie Groenland., 1954.

Hills, B. H., Harper, J. T., Humphrey, N. F. and Meierbachtol, T. W.: Measured Horizontal Temperature Gradients Constrain Heat Transfer Mechanisms in Greenland Ice, Geophys. Res. Lett., 44(19), 9778–9785, https://doi.org/10.1002/2017GL074917, 2017.

Hills, B. H., Harper, J. T., Meierbachtol, T. W., Johnson, J. V., Humphrey, N. F. and Wright, P. J.: Processes influencing heat transfer in the near-surface ice of Greenland ' s ablation zone, The Cryosphere, 12, 3215–3227, https://doi.org/10.5194/tc-12-3215-2018, 2018.

Hirashima, H., Yamaguchi, S., Sato, A., and Lehning, M.: Numerical modeling of liquid water movement through layered snow based on new measurements of the water retention curve, Cold Reg. Sci. Technol., 64, 94–103, https://doi.org/10.1016/j.coldregions.2010.09.003, 2010.

Hofer, S., Tedstone, A.J., Fettweis, X. and Bamber, J.L.: Decreasing cloud cover drives the recent mass loss on the Greenland ice sheet. Science Advances, 3(6), p.e1700584, https://doi.org/10.1126/sciadv.1700584, 2017.

Hooke, R. L.: Near-surface temperature in the superimposed ice zone and lower part of the soaked zone of polar ice sheets, J. Glaciol., https://doi.org/10.3189/S0022143000031695, 1974.

Hooke, R. L.: Pleistocene ice at the base of the Barnes ice cap, Baffin island, N.W.T. Canada, J. Glaciol., 17(75), https://doi.org/10.3189/S0022143000030719, 1976.

Horlings, A. N., Christianson, K., & Miège, C.: Expansion of firn aquifers in southeast Greenland. Journal of Geophysical Research: Earth Surface, 127, e2022JF006753. https://doi.org/10.1029/2022JF006753, 2022.

How, P.; Abermann, J.; Ahlstrøm, A.P.; Andersen, S.B.; Box, J. E.; Citterio, M.; Colgan, W.T.; Fausto. R.S.; Karlsson, N.B.; Jakobsen, J.; Langley, K.; Larsen, S.H.; Mankoff, K.D.; Pedersen, A.Ø.; Rutishauser, A.; Shield, C.L.; Solgaard, A.M.; van As, D.; Vandecrux, B.; Wright, P.J., 2022: PROMICE and GC-Net automated weather station data in Greenland, https://doi.org/10.22008/FK2/IW73UU, GEUS Dataverse, 2022.

Humphrey, N. F., Harper, J. T. and Pfeffer, W. T.: Thermal tracking of meltwater retention in Greenland's accumulation area, J. Geophys. Res. Earth Surf., 117(F1), https://doi.org/10.1029/2011JF002083, 2012.

Humphrey, N., Harper, J., and Meierbachtol, T.: Physical limits to meltwater penetration in firn. *Journal of Glaciology, 67*(265), 952-960. https://doi.org/10.1017/jog.2021.44, 2021.

IPCC: IPCC Special Report on the Ocean and Cryosphere in a Changing Climate. https://www.ipcc.ch/srocc/, 2019.

Kingma, D.P. and Ba, J.: Adam: A method for stochastic optimization. *arXiv preprint arXiv:1412.6980*, 2014.

Kjær, H. A., Zens, P., Edwards, R., Olesen, M., Mottram, R., Lewis, G., Terkelsen Holme, C., Black, S., Holst Lund, K., Schmidt, M., Dahl-Jensen, D., Vinther, B., Svensson, A., Karlsson, N., Box, J., Kipfstuhl, S. and Vallelonga, P.: Recent North Greenland temperature warming and accumulation, Cryosph. Discuss., (January), 1–27, https://doi.org/10.5194/tc-2020-337, 2021.

Koch, J.P., and Wegener, A.: Wissenschaftliche Ergebnisse Der Dänischen Expedition Nach Dronning Louises-Land Und Quer über Das Inlandeis Von Nordgrönland 1912 - 13 Unter Leitung Von Hauptmann J. P. Koch : 1., 1930.

Kuipers Munneke, P., van den Broeke, M. R., Reijmer, C. H., Helsen, M. M., Boot, W., Schneebeli, M., and Steffen, K.:
720   The role of radiation penetration in the energy budget of the snowpack at Summit, Greenland, The Cryosphere, 3, 155–165,
https://doi.org/10.5194/tc-3-155-2009, 2009.

Kuipers Munneke, P., Ligtenberg, S. R. M., van den Broeke, M. R., van Angelen, J. H., and Forster, R. R.: Explaining
the presence of perennial liquid water bodies in the firn of the Greenland ice sheet, Geophys. Res. Lett., 41, 476–483,
https://doi.org/10.1002/2013GL058389, 2014.

725   Lance, G.N. and Williams, W.T.: Mixed-Data Classificatory Programs I - Agglomerative Systems. Australian Computer
Journal, 1(1), pp.15-20, 1967.

Langen, P.L., Fausto, R.S., Vandecrux, B., Mottram, R.H. and Box, J.E.: Liquid Water Flow and Retention on the
Greenland Ice Sheet in the Regional Climate Model HIRHAM5: Local and Large-Scale Impacts. Front. Earth Sci. 4:110.
https://doi.org/10.3389/feart.2016.00110, 2017

730   Langway, C.C.: Accumulation and Temperature on The Inland Ice of North Greenland, 1959, J. Glaciol., 3(30), 1017–
1044, https://doi.org/10.3189/s0022143000017433, 1961.

Laternser, M.: Firn temperature and snow pit studies on the EGIG eastern traverse of central Greenland, 1992. Zürich,
Eidgenössische Technische Hochschute. Versuchsanstalt Kur Wasserbau, Hydrologie und Glaziologie. (Arbeitsheft 15.),
1994.

735   Law, R., Christoffersen, P., Hubbard, B., Doyle, S. H., Chudley, T. R., Schoonman, C. M., Bougamont, M., des Tombe,
B., Schilperoort, B., Kechavarzi, C., Booth, A. and Young, T. J.: Thermodynamics of a fast-moving Greenlandic outlet
glacier   revealed   by   fiber-optic   distributed   temperature   sensing,   Sci.   Adv.,   7(20),   7136–7150,
https://doi.org/10.1126/sciadv.abe7136, 2021.

Ligtenberg, S. R. M., Helsen, M. M., and van den Broeke, M. R.: An improved semi-empirical model for the
740   densification of Antarctic firn, The Cryosphere, 5, 809–819, https://doi.org/10.5194/tc-5-809-2011, 2011.

Ligtenberg, S. R. M., Kuipers Munneke, P., Noël, B. P. Y., and van den Broeke, M. R.: Brief communication: Improved
simulation of the present-day Greenland firn layer (1960–2016), The Cryosphere, 12, 1643–1649, https://doi.org/10.5194/tc-
12-1643-2018, 2018.

Liu, Q., Niu, J., Lu, P., Dong, F., Zhou, F., Meng, X., Xu, W., Li, S. and Hu, B.X.: Interannual and seasonal variations of
745   permafrost thaw depth on the Qinghai-Tibetan plateau: A comparative study using long short-term memory, convolutional
neural   networks,   and   random   forest.   *Science   of   The   Total   Environment*,   *838*,   p.155886,
https://doi.org/10.1016/j.scitotenv.2022.155886, 2022.

Lorentzen, M., Bredesen, K., Mosegaard, K. and Nielsen, L.: Estimation of shear sonic logs in the heterogeneous and
fractured Lower Cretaceous of the Danish North Sea using supervised learning. *Geophysical Prospecting*, 70, 1410– 1431.
750   https://doi.org/10.1111/1365-2478.13252, 2022.

Lundin, J. M. D., Stevens, C. M., Arthern, R., Buizert, C., Orsi, A., Ligtenberg, S. R. M., Simonsen, S. B., Cummings, E., Essery, R., Leahy, W., Harris, P., Helsen, M. M., and Waddington, E. D.: Firn Model Intercomparison Experiment (FirnMICE), J. Glaciol., 63, 401–422, https://doi.org/10.1017/jog.2016.114, 2017.

755   Lüthi, M. P., Ryser, C., Andrews, L. C., Catania, G. A., Funk, M., Hawley, R. L., Hoffman, M. J. and Neumann, T. A.: Heat sources within the Greenland ice sheet: Dissipation, temperate paleo-firn and cryo-hydrologic warming, The Cryosphere, 9(1), 245–253, https://doi.org/10.5194/tc-9-245-2015, 2015.

Løkkegaard, A., Mankoff, K., Zdanowicz, C., Clow, G. D., Lüthi, M. P., Doyle, S., Thomsen, H., Fisher, D., Harper, J., Aschwanden, A., Vinther, B. M., Dahl-Jensen, D., Zekollari, H., Meierbachtol, T., McDowell, I., Humphrey, N., Solgaard, A., Karlsson, N. B., Khan, S. A., Hills, B., Law, R., Hubbard, B., Christoffersen, P., Jacquemart, M., Fausto, R. S., and

760   Colgan, W. T.: Greenland and Canadian Arctic ice temperature profiles, The Cryosphere Discuss. [preprint], https://doi.org/10.5194/tc-2022-138, in review, 2022.

Machguth, H., MacFerrin, M., van As, D., Box, J.E., Charalampidis, C., Colgan, W., Fausto, R.S., Meijer, H.A., Mosley-Thompson, E. and van de Wal, R.S. Greenland meltwater storage in firn limited by near-surface ice formation. *Nature Clim Change* **6,** 390–393, https://doi.org/10.1038/nclimate2899, 2016.

765   Mankoff, K., Løkkegaard, A., Colgan, W., Thomsen, H., Clow, G., Fisher, D., Zdanowicz, C., Lüthi, M.P., Vinther, B., MacGregor, J.A., McDowell, I., Zekollari, H., Meierbachtol, T., Doyle, S., Law, R., Hills, B., Harper, J., Humphrey, N., Hubbard, B., Christoffersen, P., Jacquemart, M.: Greenland deep ice temperature database, https://doi.org/10.22008/FK2/3BVF9V, GEUS Dataverse, V1, 2022.

Mattingly, K. S., Mote, T. L., and Fettweis, X.: Atmospheric river impacts on Greenland ice sheet surface mass balance.

770   Journal of Geophysical Research, 123(16), 8538–8560. https://doi.org/10.1029/2018jd028714, 2018.

Thompson-Munson, M., Montgomery, L., Lenaerts, J., and Koenig, L.: Surface Mass Balance and Snow Depth on Sea Ice Working Group (SUMup) 10 meter borehole temperature subdataset, Greenland and Antarctica, 1957-2017, Arctic Data Center, http://doi.org/https://doi.org/10.18739/A2DB7VR1P, 2022.

Meier, M. F., Conel, J. E., Hoerni, J. A., Melbourne, W. G., and Pings, C. J.: Preliminary Study of Crevasse Formation.

775   Blue Ice Valley, Greenland, 1955. U. S. Army Snow Ice and Permafrost Research Establishment, Corps of Engineers, Report 38, 80 pp., 1957.

MacFerrin, M., Machguth, H., As, D.V., Charalampidis, C., Stevens, C.M., Heilig, A., Vandecrux, B., Langen, P.L., Mottram, R., Fettweis, X. and van den Broeke, M.R.: Rapid expansion of Greenland's low-permeability ice slabs. *Nature*, *573*(7774), pp.403-407, https://doi.org/10.1038/s41586-019-1550-3, 2019.

780   MacFerrin, M., Stevens, C. M., and Vandecrux, B.: The Greenland Firn Compaction Verification and Reconnaissance (FirnCover) Dataset, 2013-2019. Arctic Data Center. https://doi.org/10.18739/A25X25D7M. 2021.

MacFerrin, M. J., Stevens, C. M., Vandecrux, B., Waddington, E. D., and Abdalati, W.: The Greenland Firn Compaction Verification and Reconnaissance (FirnCover) dataset, 2013–2019, Earth Syst. Sci. Data, 14, 955–971, https://doi.org/10.5194/essd-14-955-2022, 2022.

785   Marshall S.J.: Regime Shifts in Glacier and Ice Sheet Response to Climate Change: Examples From the Northern Hemisphere, Front. Clim., 3:702585, https://doi.org/10.3389/fclim.2021.702585, 2021.

Matoba, S., Motoyama, H., Fujita, K., Yamasaki, T., Minowa, M., Onuma, Y., Komuro, Y., Aoki, T., Yamaguchi, S., Sugiyama, S. and Enomoto, H.: Glaciological and meteorological observations at the SIGMA-D site, northwestern Greenland ice sheet, Bull. Glaciol. Res., 33, 7–14, https://doi.org/10.5331/bgr.33.7, 2015.

790   McGrath, D., Colgan, W., Bayou, N., Muto, A. and Steffen, K.: Recent warming at Summit, Greenland: Global context and implications, Geophys. Res. Lett., 40(10), 2091–2096, https://doi.org/10.1002/grl.50456, 2013.

Meyer, H. and Pebesma, E.: Predicting into unknown space? Estimating the area of applicability of spatial prediction models. Methods in Ecology and Evolution, 12(9), pp.1620-1633, https://doi.org/10.1111/2041-210X.13650, 2021.

Miller, N. B., Shupe, M. D., Cox, C. J., Noone, D., Persson, P. O. G., and Steffen, K.: Surface energy budget responses to
795   radiative forcing at Summit, Greenland, The Cryosphere, 11, 497–516, https://doi.org/10.5194/tc-11-497-2017, 2017.

Miller, O., Solomon, D. K., Miège, C., Koenig, L., Forster, R., Schmerr, N., Ligtenberg, S. R. M., Legchenko, A., Voss, C. I., Montgomery, L. and McConnell, J. R.: Hydrology of a Perennial Firn Aquifer in Southeast Greenland: An Overview Driven by Field Data, Water Resour. Res., 56(8), e2019WR026348, https://doi.org/10.1029/2019WR026348, 2020.

Mock, S. J.: Glaciological studies in the vicinity of Camp Century, Greenland, , U.S. Army Cold Region Research and
800   Engineering Report n.157 [online] Available from: https://hdl.handle.net/11681/5774 (Accessed 26 August 2022), 1965

Mock, S. J. and Weeks, W.F.: The distribution of ten-meter snow temperatures on the Greenland ice sheet, U.S. Army Cold Region Research and Engineering Report n.157 [online] Available from: https://hdl.handle.net/11681/5730 (Accessed 26 August 2022), 1965.

Mock, S. J. and Ragle, R. H.: Elevations on the ice sheet of southern Greenland, U.S. Army Cold Region Research and
805   Engineering Report n.124 [online] Available from: http://hdl.handle.net/11681/5624 (last access 26 August 2022), 1963.

Muñoz Sabater, J.: ERA5-Land monthly averaged data from 1950 to present. Copernicus Climate Change Service (C3S) Climate Data Store (CDS). https://doi.org/10.24381/cds.68d2bb30, 2019.

Nobles, L. H., Glaciological investigations, Nunatarssuaq ice ramp, Northwestern Greenland, Tech. Rep. 66, U.S. Army Snow, Ice and Permafrost Research Establishment, Corps of Engineers, [online] Available from
810   https://hdl.handle.net/11681/6030 (last access 26 August 2022), 1960.

Noël, B., van de Berg, W. J., Lhermitte, S. and van den Broeke, M. R.: Rapid ablation zone expansion amplifies north Greenland mass loss, Sci. Adv., 5(9), 2–11, https://doi.org/10.1126/sciadv.aaw0123, 2019.

Ohmura, A., Steffen, K., Blatter, H., Greuell, W., Rotach, M., Stober, M., Konzelmann, T., Forrer, J., Abe-Ouchi, A., Steiger, D. and Niederbaumer, G.: Energy and mass balance during the melt season at the equilibrium line altitude.
815   Paakitsoq, Greenland ice sheet: Progress report, 2, 1992.

Pfeffer, W. T., Meier, M. F. and Illangasekare, T. H.: Retention of Greenland runoff by refreezing: implications for projected future sea level change, J. Geophys. Res., 96(C12), 22117, https://doi.org/10.1029/91jc02502, 1991.

Phillips, T., Rajaram, H. and Steffen, K.: Cryo - hydrologic warming : A potential mechanism for rapid thermal response of ice sheets, , 37(September), 1–5, https://doi.org/10.1029/2010GL044397, 2010.

820   Phillips, T., Rajaram, H., Colgan, W., Steffen, K. and Abdalati, W.: Evaluation of cryo-hydrologic warming as an explanation for increased ice velocities in the wet snow zone, Sermeq Avannarleq, West Greenland, J. Geophys. Res. Earth Surf., 118(3), 1241–1256, https://doi.org/10.1002/jgrf.20079, 2013.

Polashenski, C., Courville, Z., Benson, C., Wagner, A., Chen, J., Wong, G., Hawley, R. and Hall, D.: Observations of pronounced Greenland ice sheet firn warming and implications for runoff production, Geophys. Res. Lett., 41(12), 4238–

825   4246, https://doi.org/10.1002/2014GL059806, 2014.

de Quervain, M.: Schneckundliche Arbeiten der Internat. Glaziolog. Gronlandexpedition., Meddelelser om Gronl., 177(4), 1969.

Ragle, R. H. and Davis, T. C.: South Greenland traverses, J. Glaciol., 4(31), 129–131, https://doi.org/10.3189/s002214300001830x, 1962.

830   Rantanen, M., Karpechko, A.Y., Lipponen, A., Nordling, K., Hyvärinen, O., Ruosteenoja, K., Vihma, T. and Laaksonen, A.: The Arctic has warmed nearly four times faster than the globe since 1979. Nature Communications Earth & Environment, 3(1), p.168, https://doi.org/10.1038/s43247-022-00498-3, 2022.

Rinker, J. and Mock, S.: Radar Ice Thickness Profiles: Northwest Greenland, CRREL Spec. Rep., 103 [online] Available from: http://hdl.handle.net/11681/11861 (last access 26 August 2022), 1967.

835   Rumelhart, D. E., G. E. Hinton, and R. J. Williams: Learning representations by backpropagating errors. Nature, 323 (6088), 533–536, https://doi.org/10.1038/323533a0, URL https://doi.org/10.1038/323533a0, 1986.

Ryan, J. C., Smith, L. C., As, D. Van, Cooley, S. W., Cooper, M. G., Pitcher, L. H. and Hubbard, A.: Greenland ice sheet surface melt amplified by snowline migration and bare ice exposure, , 1–11, https://doi.org/10.1126/sciadv.aav373, 2019.

Ryan, J.C., Smith, L.C., Cooley, S.W. *et al.* Decreasing surface albedo signifies a growing importance of clouds for

840   Greenland Ice Sheet meltwater production. *Nat Commun* **13**, 4205, https://doi.org/10.1038/s41467-022-31434-w, 2022.

Samimi, S., Marshall, S. J., Vandecrux, B., and MacFerrin, M.: Time-domain reflectometry measurements and modeling of firn meltwater infiltration at DYE-2, Greenland. Journal of Geophysical Research: Earth Surface, 126, e2021JF006295. https://doi.org/10.1029/2021JF006295, 2021.

Schwager, M.: Eisbohrkernuntersuchungen, Ber. Polarforsch, 362, 2000.

845   Schytt, V.: Glaciological investigations in the Thule Ramp area, U. S. Army Snow Ice and Permafrost Research Establishment, Corps of Engineers, Report 28, 88 pp., http://hdl.handle.net/11681/5981, 1955.

Smeets, P. C. J. P. Kuipers Munneke, P., van As, D., van den Broeke, M. R., Boot, W., Oerlemans, H., Snellen, H., Reijmer, C. H. and van de Wal, R. S. W.: The K-transect in west Greenland: Automatic weather station data (1993–2016), Arctic, Antarctic, and Alpine Research, 50:1, https://doi.org/10.1080/15230430.2017.1420954, 2018.

850   Sorge, E.: Glaziologische Untersuchungen in Eismitte, in K. Wegener: Wissenschaftliche Ergebnisse der Deutschen Grönlandexpedition Alfred Wegener 1929 und 1930/1931., F. A. Brockhaus, Vol. 3, 1935.

Stauffer, B. and Oeschger, H.: Temperaturprofile in Bohrlöchern am Rande des grönländischen Inlandeises. Mitteilungen der Versuchsanstalt für Wasserbau, Hydrologie und Glaziologie an der Eidgenössischen Technischen Hochschule (Zürich) 41: 301—313, 1979.

855   Steffen, K., Box, J., Abdalati,W. : Greenland Climate Network: GC-Net, in Glaciers, Ice Sheets and Volcanoes: A Tribute to Mark F. Meier, S, Ed.: C. Colbeck, Special Report, Cold Regions Research and Engineering Laboratory, 1996.

Steffen, K., and Box, J.: Surface climatology of the Greenland ice sheet: Greenland Climate Network 1995–1999, J. Geophys. Res., 106(D24), 33951– 33964, https://doi.org/10.1029/2001JD900161, 2001.

Steger, C. R., Reijmer, C. H., and van den Broeke, M. R.: The modelled liquid water balance of the Greenland Ice Sheet,
860   The Cryosphere, 11, 2507–2526, https://doi.org/10.5194/tc-11-2507-2017, 2017.

Steiner, D., Walter, A., and Zumbühl, H.: The application of a non-linear back-propagation neural network to study the mass balance of Grosse Aletschgletscher, Switzerland. Journal of Glaciology, 51(173), 313-323. https://doi.org/10.3189/172756505781829421, 2005.

Stibal, M., Box, J. E., Cameron, K. A., Langen, P. L., Yallop, M. L., Mottram, R. H., Khan, A. L., Molotch, N. P.,
865   Chrismas, N. A. M., Calì Quaglia, F., Remias, D., Smeets, C. J. P. P., van den Broeke, M. R., Ryan, J. C., Hubbard, A., Tranter, M., van As, D. and Ahlstrøm, A. P.: Algae Drive Enhanced Darkening of Bare Ice on the Greenland ice sheet, Geophys. Res. Lett., 44(22), 11,463-11,471, https://doi.org/10.1002/2017GL075958, 2017.

Tedstone, A.J., Machguth, H. Increasing surface runoff from Greenland's firn areas. *Nat. Clim. Chang.* **12,** 672–676: https://doi.org/10.1038/s41558-022-01371-z, 2022.

870   Thomsen, H. ., Olesen, O. ., Braithwaite, R. . and Bøggild, C. .: Ice drilling and mass balance at Pâkitsoq, Jakobshavn, central West Greenland, Rapp. Grønlands Geol. Undersøgelse, 152, 80–84, https://doi.org/10.34194/rapggu.v152.8160, 1991.

Thomsen, H. ., Reeh, N., Olesen, O. . and Jonsson, P.: Glacier and climate research on Hans Tausen Iskappe, North Greenland – 1995 glacier basin activities and preliminary results, Bull. Grønlands Geol. Undersøgelse, 172, 78–84,
875   https://doi.org/10.34194/bullggu.v172.6749, 1996.

Trusel, L.D., Das, S.B., Osman, M.B., Evans, M.J., Smith, B.E., Fettweis, X., McConnell, J.R., Noël, B.P. and van den Broeke, M.R.: Nonlinear rise in Greenland runoff in response to post-industrial Arctic warming. Nature, 564(7734), pp.104-108, https://doi.org/10.1038/s41586-018-0752-4, 2018.

Tsutaki, S., Sugiyama, S., Sakakibara, D., Aoki, T. and Niwano, M.: Surface mass balance, ice velocity and near-surface
880   ice temperature on Qaanaaq Ice Cap, northwestern Greenland, from 2012 to 2016, Ann. Glaciol., 58(75), 181–192, https://doi.org/10.1017/aog.2017.7, 2017.

U.S. Army Transportation Board: Report of environmental operation: Lead Dog 1960, Final Report, Project Lead Dog, TCB- 60 - 023 - E0, 188p. https://apps.dtic.mil/sti/pdfs/AD0263548.pdf, 1960.

Van Dalum, C. T., Jan Van De Berg, W. and Van Den Broeke, M. R.: Impact of updated radiative transfer scheme in snow and ice in RACMO2.3p3 on the surface mass and energy budget of the Greenland ice sheet, The Cryosphere, 15(4), 1823–1844, https://doi.org/10.5194/tc-15-1823-2021, 2021.

Vandecrux, B., MacFerrin, M., Machguth, H., Colgan, W. T., van As, D., Heilig, A., Stevens, C. M., Charalampidis, C., Fausto, R. S., Morris, E. M., Mosley-Thompson, E., Koenig, L., Montgomery, L. N., Miège, C., Simonsen, S. B., Ingeman-Nielsen, T., and Box, J. E.: Firn data compilation reveals widespread decrease of firn air content in western Greenland, The Cryosphere, 13, 845–859, https://doi.org/10.5194/tc-13-845-2019, 2019.

Vandecrux, B., Fausto, R. S., Van As, D., Colgan, W., Langen, P. L., Haubner, K., Ingeman-Nielsen, T., Heilig, A., Stevens, C. M., MacFerrin, M., Niwano, M., Steffen, K. and Box, J. E.: Firn cold content evolution at nine sites on the Greenland ice sheet between 1998 and 2017, J. Glaciol., 66(258), 591–602, https://doi.org/10.1017/jog.2020.30, 2020a.

Vandecrux, B., Mottram, R., Langen, P. L., Fausto, R. S., Olesen, M., Stevens, C. M., Verjans, V., Leeson, A., Ligtenberg, S., Kuipers Munneke, P., Marchenko, S., van Pelt, W., Meyer, C. R., Simonsen, S. B., Heilig, A., Samimi, S., Marshall, S., Machguth, H., MacFerrin, M., Niwano, M., Miller, O., Voss, C. I., and Box, J. E.: The firn meltwater Retention Model Intercomparison Project (RetMIP): evaluation of nine firn models at four weather station sites on the Greenland ice sheet, The Cryosphere, 14, 3785–3810, https://doi.org/10.5194/tc-14-3785-2020, 2020b.

Vandecrux, B., Colgan, W., Solgaard, A.M., Steffensen, J.P., and Karlsson, N.B.(2021). Firn evolution at Camp Century, Greenland: 1966-2100, Frontiers in Earth Science, https://doi.org/10.3389/feart.2021.578978, 2021

Vandecrux, B., Box, J. E., Ahlstrøm, A. P., Andersen, S. B., Bayou, N., Colgan, W. T., Cullen, N. J., Fausto, R. S., Haas-Artho, D., Heilig, A., Houtz, D. A., How, P., Iosifescu Enescu, I., Karlsson, N. B., Kurup Buchholz, R., Mankoff, K. D., McGrath, D., Molotch, N. P., Perren, B., Revheim, M. K., Rutishauser, A., Sampson, K., Schneebeli, M., Starkweather, S., Steffen, S., Weber, J., Wright, P. J., Zwally, H. J., and Steffen, K.: The historical Greenland Climate Network (GC-Net) curated and augmented Level 1 dataset, Earth Syst. Sci. Data Discuss. [preprint], https://doi.org/10.5194/essd-2023-147, in review, 2023.

Vandecrux, B.: Greenland ice sheet 10 m subsurface temperature compilation 1912-2022, https://doi.org/10.22008/FK2/TURMGZ, GEUS Dataverse, V1, 2023a.

Vandecrux, B.: Greenland ice sheet 10 m ice and firn temperature reconstruction, 1950-2022, https://doi.org/10.22008/FK2/C24WVN, GEUS Dataverse, V2, 2023b.

Vandecrux, B.: Greenland ice sheet subsurface temperature compilation scripts (v1.0). Zenodo. https://doi.org/10.5281/zenodo.8027442, 2023c.

Van Den Broeke, M., Smeets, P., Ettema, J., Van Der Veen, C., Van De Wal, R. and Oerlemans, J.: Partitioning of melt energy and meltwater fluxes in the ablation zone of the west Greenland ice sheet, The Cryosphere, 2(2), 179–189, https://doi.org/10.5194/tc-2-179-2008, 2008.

Van Den Broeke, M. R., Enderlin, E. M., Howat, I. M., Kuipers Munneke, P., Noël, B. P. Y., Jan Van De Berg, W., Van Meijgaard, E. and Wouters, B.: On the recent contribution of the Greenland ice sheet to sea level change, The Cryosphere, 10(5), 1933–1946, https://doi.org/10.5194/tc-10-1933-2016, 2016.

Van der Veen, C. J., Jezek, K. C., Whillans, I. M., Bolzan, J. F. and Mosley-Thompson, E.: Two decades of glaciological investigations in South and Central Greenland, Polar Geogr., 24(4), 259–349, https://doi.org/10.1080/10889370009377700, 2000.

Vionnet, V., Brun, E., Morin, S., Boone, A., Faroux, S., Le Moigne, P., Martin, E., and Willemet, J.-M.: The detailed snowpack scheme Crocus and its implementation in SURFEX v7.2, Geosci. Model Dev., 5, 773–791, https://doi.org/10.5194/gmd-5-773-2012, 2012.

Weertman, J.: Comparison between measured and theoretical temperature profiles of the Camp Century, Greenland, Borehole, J. Geophys. Res., 73(8), https://doi.org/10.1029/JB073i008p02691, 1968.

Wang, W., Zender, C. S., van As, D., Fausto, R. S., and Laffin, M. K.: Greenland surface melt dominated by solar and sensible heating. Geophysical Research Letters, 48, e2020GL090653. https://doi.org/10.1029/2020GL090653, 2021.

Wegener, A.: Deutsche Grönland- Expedition Alfred Wegener : ausgeführt unter der Leitung von Alfred Wegener und Kurt Wegener 1929 und 1930/1931 : wissenschaftliche Ergebnisse., 1935.

Wiscombe, W. J. and Warren, S. G.: A model for the spectral albedo of snow. I: pure snow., J. Atmos. Sci., 37(12), 2712–2733, https://doi.org/10.1175/1520-0469(1980)037<2712:AMFTSA>2.0.CO;2, 1980.

Xiong, Z., Cui, Y., Liu, Z., Zhao, Y., Hu, M. and Hu, J.: Evaluating explorative prediction power of machine learning algorithms for materials discovery using k-fold forward cross-validation. *Computational Materials Science*, *171*, p.109203, https://doi.org/10.1016/j.commatsci.2019.109203, 2020.

Xu, W., Balaguru, K., August, A., Lalo, N., Hodas, N., DeMaria, M., and Judi, D.: Deep Learning Experiments for Tropical Cyclone Intensity Forecasts. *Wea. Forecasting*, **36**, 1453–1470, https://doi.org/10.1175/WAF-D-20-0104.1, 2021.

Yamaguchi, S., Matoba, S., Yamazaki, T., Tsushima, A., Niwano, M., Tanikawa, T. and Aoki, T.: Glaciological observations in 2012 and 2013 at SIGMA-A site, Northwest Greenland, Bull. Glaciol. Res., 32(1), 95–105, https://doi.org/10.5331/bgr.32.95, 2014.

Yen, Y.-C.: Review of thermal properties of snow, ice and sea ice, CRREL Report 81-10, 1–27, available at: https://usace.contentdm.oclc.org/digital/api/collection/p266001coll1/id/7366/download (last access: 2 November 2020), 1981.

Zhang, Q., Huai, B., van den Broeke, M. R., Cappelen, J., Ding, M., Wang, Y., and Sun, W.: Temporal and spatial variability in contemporary Greenland warming (1958-2020), Journal of Climate, 2022, https://doi.org/10.1175/JCLI-D-21-0313.1, 2022.

Zwally, H. Jay, Mario B. Giovinetto, Matthew A. Beckley, and Jack L. Saba,: Antarctic and Greenland Drainage Systems, GSFC Cryospheric Sciences Laboratory, at http://icesat4.gsfc.nasa.gov/cryo_data/ant_grn_drainage_systems.php, 2012.